universität wien

MASTERARBEIT / MASTER'S THESIS

Titel der Masterarbeit / Title of the Master's Thesis

Discovery and Characterization of the Interaction between Calcineurin and Myotilin

verfasst von / submitted by

Tamara Sijacki, BSc

angestrebter akademischer Grad / in partial fulfilment of the requirements for the degree of

Master of Science (MSc)

Wien, 2019 / Vienna 2019

Studienkennzahl lt. Studienblatt / degree programme code as it appears on the student record sheet:	A 066 834
Studienrichtung lt. Studienblatt / degree programme as it appears on the student record sheet:	Masterstudium Molekulare Biologie
Betreut von / Supervisor:	Univ.-Prof. Dipl.-Ing. Dr. Kristina Djinovic-Carugo

Acknowledgements

Firstly, I would like to thank my supervisor, Univ.-Prof. Dipl.-Ing. Dr. Kristina Djinović-Carugo, for letting me work on this exciting, new discovery. Although it started as a small project, she gave me the freedom to expand it and shape it by exploring my own ideas.

Next, I want to express my deepest gratitude to Mag. Julius Kostan, PhD, who was my mentor in the lab. He was always there to make me excited about the project on the days I needed motivation, but also to provide valuable advice and constructive criticism when it was needed. Finally, Julius taught me the importance of stepping back and seeing the bigger picture of one's project and enjoying the daily lab work.

Thanks is due to Antonio Sponga, MSc, for sharing the CN purification protocol, teaching me how to use crystallization robots and offering advice throughout this project. I would also like to acknowledge Ing. Claudia Schreiner, who worked on the project and contributed to our findings, and Amelie Schönenwald, MSc, who diffracted the CN-myotilin crystals at ESRF. Special thanks go to Dipl.-Ing. Dr. Dalibor Milić, who taught me how to solve the structure presented in this work and gladly helped me with model building along the way. I learned a lot from our interesting discussions.

Finally, I cannot end without thanking all my other colleagues from the Djinović lab for all the funny moments we shared while working or having a short candy break. The amount of support and optimism from every single one of them motivated me to work harder and made me start and finish each day at the lab with a smile.

Abstract

The Z-disc is an intricate assembly of over 40 different proteins, which coordinates forces from different sarcomeres to give rise to a controlled, unidirectional contraction. Myotilin is an important component of this complex best known for its ability to organize filamentous actin (F-actin). In addition, myotilin binds and stabilizes other Z-disc proteins on F-actin. Myotilin is a target of extensive research, as point mutations of myotilin trigger disorganization of sarcomeres and harmful protein aggregation that cause severe myopathies. Although several studies have alluded to its dynamic nature and complex regulation through post-translational modifications, its function beyond F-actin binding remains poorly understood. In this study, we identified myotilin as a new substrate of calcineurin (CN), a Ca2+ dependent Ser/Thr phosphatase, which activates muscle hypertrophy, fiber remodeling, repair or muscle degradation.

Firstly, by using pulldown assays, we showed that myotilin can directly interact with CN. Secondly, by using CelluSpots overlay assays, we identified a region of myotilin containing a sequence resembling the LxVP motif, one of the two established substrate recognition motifs of CN, to be involved in this interaction. Next, we crystallized CN in complex with a myotilin peptide and determined its structure at 2.77 Å, which unambiguously showed myotilin to interact with CN via its LxVP motif. In addition, by using ITC, we found the affinity of myotilin to CN to be in micromolar range, typical for CN substrates. Finally, dephosphorylation assays performed with phosphorylated peptides of myotilin showed that CN is able to dephosphorylate three serine residues of myotilin, namely Ser229, Ser231 and Ser233 in vitro.

Altogether, our findings allude to a more complex mechanism of myotilin regulation. We speculate that the 30 residue long stretch of myotilin spanning from the LxVP motif to the first Ig domain could be a hot-spot of myotilin regulation. Although myotilin was recently reported to have a more dynamic function as a major marker of muscle remodeling in exercise induced muscle lesions, little is known about its regulation. Our findings could be used as a starting point of investigating these important processes, as CN could be the enzyme which drives myotilin turnover at the Z-disc and its recruitment to the sites of muscle lesion.

Zusammenfassung

Die Z-Scheibe ist ein komplexes Netzwerk bestehend aus mehr als 40 verschiedenen Proteinen, welches die Generation einer kontrollierten, unidirektionalen Kontraktion koordiniert. Myotilin, ein wichtiger Bestandteil dieses Netzwerks, organisiert Aktinfilamente, außerdem verankert und stabilisiert es andere Proteine der Z-Scheibe auf Aktinfilamenten. Myotilin steht im Zentrum zahlreicher Studien, da Punktmutationen in Myotilin zum Ordnungsverlust in Sarkomeren und zur Ansammlung schädlicher Proteinaggregate führen, welche schwere Myopathien verursachen. Obwohl das dynamische Verhalten und die komplexe Regulierung von Myotilin durch post-translationale Modifikation vielfach untersucht wurden, ist bis heute nicht bekannt, welche Rolle es neben der Interaktion mit Aktin spielt. In dieser Arbeit haben wir entdeckt, dass Myotilin ein Substrat von Calcineurin (CN) ist, eine Ca^{2+}-abhängige Ser/Thr-Phosphatase, welche Muskelhypertrophie, Faser-Remodelling, Muskelregeneration und Muskelabbau aktiviert.

Durch Pulldown-Assays konnten wir zeigen, dass Myotilin direct mit CN interagieren kann. Mithilfe von CelluSpots Overlay Assays haben wir die Region in Myotilin bestimmt, welche an dieser Interaktion beteiligt ist. Diese Region enthält eine Sequenz, welche dem LxVP-Motiv ähnelt, eines von zwei kanonischen Substraterkennungsmotiven von CN. Wir konnten die Kristallstruktur eines Komplexes, bestehend aus CN und einem Myotilin-Peptid, mit einer Auflösung von 2.77 Å bestimmen. Dadurch konnten wir bestätigen, dass Myotilin durch sein LxVP Motiv mit CN interagiert. Mittels Isothermaler Kalorimetrie haben wir die Affinität von Myotilin zu CN gemessen, welche - charakteristisch für CN-Substrate - im niedrigen mikromolaren Bereich liegt. Schlussendlich haben wir Desphosphorylierungs-Assays mit phosphorylierten Myotilin-Peptiden durchgeführt. Diese zeigten, dass CN in der Lage ist, Myotilin an drei verschiedenen Positionen in vitro zu dephosphorylieren, Ser229, Ser231 und Ser233.

Unsere Ergebnisse deuten auf einen komplexeren Mechanismus der Myotilin Regulation hin. Wir vermuten, dass die 30 Aminosäuren lange Region in Myotilin, welche vom LxVP Motiv bis zur ersten Ig-Domäne reicht, ein Regulations-Hotspot ist. Obwohl kürzlich berichtet wurde, dass Myotilin eine dynamische Rolle als wichtiger Marker von Muskel-Remodelling in Aktivitäts-induzierten Muskelschäden spielt, ist wenig über seine Regulierung bekannt. Diese Arbeit soll als Ansatz dienen, diese wichtigen Prozesse zu untersuchen, da CN das Enzym sein könnte, welches Myotilin-Turnover an der Z-Scheibe und seine Rekrutierung an Stellen von Muskelschäden antreibt.

Table of Contents

Introduction

Part I: Introduction to striated muscle, Z-disc and myotilin

Multiple levels of striated muscle organization

Striated muscles are amongst the most organized structures in the human body. Connective tissue separates the muscle into bundles, which are further divided into muscle fibers. These muscle fibers are unique, as each fiber represent a myocyte, one large, multinuclear cell, which is produced by fusion of individual muscle cells during development. The cell membrane which wraps around each muscle fiber, also known as the sarcolemma, creates invagination along the cell to enlarge its surface promoting information transfer and excitation-contraction coupling between neurons and muscle fibers. Each cell is composed out of specialized, contractile fibers, the myofibrils which are built out of repeating contractile units, the sarcomeres (Frontera and Ochala, 2015). Each sarcomere (Figure 1A) carries the basic contractile apparatus composed out of actin (thin filaments) and myosin (tick filaments) at its core, which give striated muscle their recognizable striped appearance of alternating dark and light bands (Frontera and Ochala, 2015; Gautel and Djinovic-Carugo, 2016; Shadrin et al., 2016).

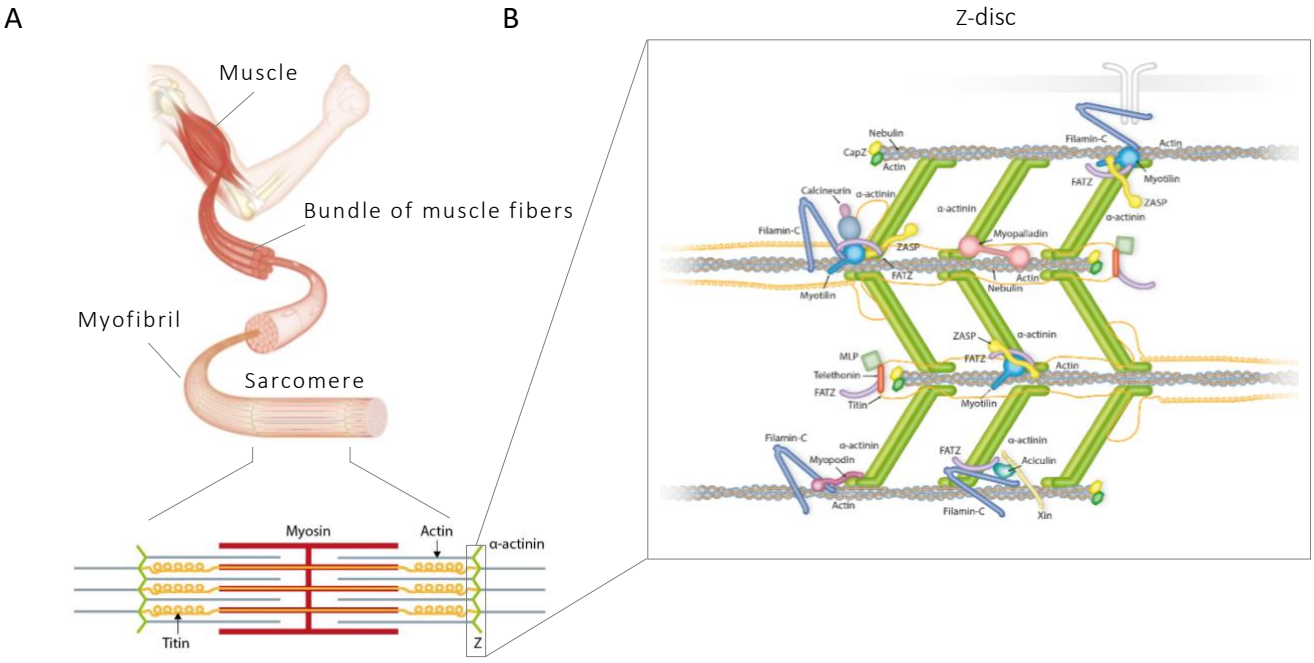

Figure 1. Structural organization of striated muscles, courtesy of the Djinovic lab.

(A) Schematic representation of the highly organized structure of striated muscles. Striated muscles are formed out of bundles of muscle fibers and each such fiber is a large multinucleated muscle cell, composed out of myofibrils. Myofibrils are built out of repeating contraction units, sarcomeres, which contract as a result of myosin-actin interaction. The borders of sarcomeres are called the Z-disc. (B) The Z-disc is a complex protein assembly composed out of numerous proteins, such as α-actinin, ZASP, FATZ, myotilin, filamin-C, teletonin, Xin, aciculin and nebulin. At the Z-disc, actin filaments from neighboring sarcomeres are kept antiparallel to each other by crosslinking proteins.

Adjacent sarcomeres are connected at their borders by a complex assembly of various proteins called the Z-disc (Figure 1B). Z-discs have an essential role in muscle contraction: because they connect actin filaments of neighboring sarcomeres and keep them arranged in an antiparallel fashion, they coordinate the force generated in individual sarcomeres. This enables constructive amplification of the force, which leads to a highly efficient unidirectional contraction product (Gautel and Djinovic-Carugo, 2016). Thus, the Z-disc is a robust structure, which keeps sarcomeres linked, and as such, plays a crucial role in assembly and later in maintenance of the sarcomere arrangement and organization, which is essential for proper contraction (Frank et al., 2006).

Actin binding proteins are a major group of Z-discs proteins

The key components of the Z-disc are a number of proteins which interact with actin. These proteins crosslink F-actin from adjacent sarcomeres and can also serve as important anchoring stations for other proteins to bind to. The Z-disc needs to be dynamic and resilient to withstand the massive strain of every contraction. Hence, no single Z-disc protein interacts with the F-actin filaments with affinities in the nM range, rather, most of them bind F-actin with affinities in low μM range (Djinovic, unpublished data), and their binding is strengthened by the interactions they establish with each other. This is crucial for efficient replacement of damaged components and prevents the Z-disc from collapsing in case of malfunction of one of its building blocks.

In the Z-disc, proteins which interact with F-actin employ several strategies to do so: nebulin is composed of specific F-actin binding repeats that wrap around F-actin (Jin and Wang, 1991), capZ interacts specifically with the barbed end of F-actin (Casella et al., 1986) and ZASP uses a ZM motif and potentially its PDZ domain to interact with F-actin (Lin et al., 2014), (Djinovic, unpublished data). Other proteins contain well-established F-actin binding domains, like the calponin-homology (CH) domain (α-actinin, filamin) (Blanchard et al., 1989; Iwamoto et al., 2018; Ribeiro Ede et al., 2014; Shizuta et al., 1976) or the immunoglobulin (Ig)-like domain (myotilin, paladin, myopalladin, titin) (Jin, 2000; Otey et al., 2009; Otey et al., 2005). The essential F-actin crosslinking protein of the Z-disc, α-actinin, interacts with F-actin via its actin binding domain (ABD) which consists of two highly similar CH domains (CH1 and CH2). In order to crosslink F-actin, α-actinin is an antiparallel homodimer which carries an ABD at each side of its rod-shaped body (Ribeiro Ede et al., 2014). Additionally, α-actinin interacts with many other Z-disc protein include nebulin (Nave et al., 1990), FATZ (Frey et al., 2000), ZASP (Faulkner et al., 1999), filamin-C , titin (Young et al., 1998) and myotilin (Salmikangas et al., 1999). Together with α-actinin, myotilin supports actin organization by cross-linking F-actin.

Myotilin is an important actin organizing protein

Myotilin (also called myofibrillar titin-like protein) is a 489 residue long, 57 kDa protein, first discovered in a yeast-two hybrid screen, where α-actinin was used as bait (Salmikangas et al., 1999). Apart from small amount of myotilin mRNA isolated from peripheral nerves, expression of myotilin is restricted specifically to the cardiac and skeletal muscle tissue, where it primarily resides in the sarcomere, specifically the Z-disc (Salmikangas et al., 1999). The first half of the protein (residues 1 to 250) does not display any structural features, and although it was shown to

contain compact regions (Djinovic, unpublished), it is characterized as being disordered (Puz et al., 2017). The only distinctive feature of this region is a unique serine-rich region located at the N-terminus, which has been reported to interact with the C-terminal region (EF-hands 3 and 4) of α-actinin (Beck et al., 2011). The second half of the protein (residues 251-498) is highly conserved and is composed out of two I-type Ig-like domains (Heikkinen et al., 2009; Puz et al., 2017), which are most homologous to Ig-like domains 4 and 5 of myopalladin, Ig domains 4 and 5 of paladin and Ig domains 7 and 8 of titin (Bang et al., 2001; Parast and Otey, 2000; Salmikangas et al., 1999).

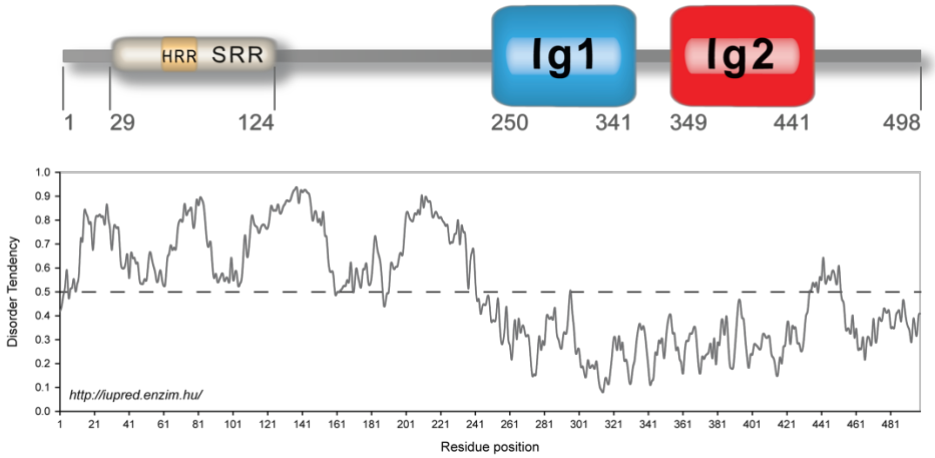

Figure 2. Schematic representation of myotilin, courtesy of the Djinovic lab.

Myotilin is a 498-residue long Z-disc protein. The protein contains a serine rich region at its N-terminal part and displays high disorder tendency from reside 1 to 250. The second half of the protein contains two Ig domains and a short disordered C-terminal tail.

Due to the high sequence homology, similar cellular localization and function, myotilin, palladin and myopalladin together form a subfamily of actin-associated proteins (Otey et al., 2005). The F-actin binding property of myotilin has been attributed to these two Ig domains. Finally, myotilin contains a short, disordered C-terminal region (Salmikangas et al., 1999).

The myotilin interactome and its interaction with actin

Like many Z-disc proteins, myotilin interacts with a plethora of other Z-disc proteins. Apart from α-actinin, its rich interactome includes ZASP (von Nandelstadh et al., 2009), FATZ (Gontier et al., 2005), filamin-C (van der Ven et al., 2000) and most significantly actin (Salmikangas et al., 2003).

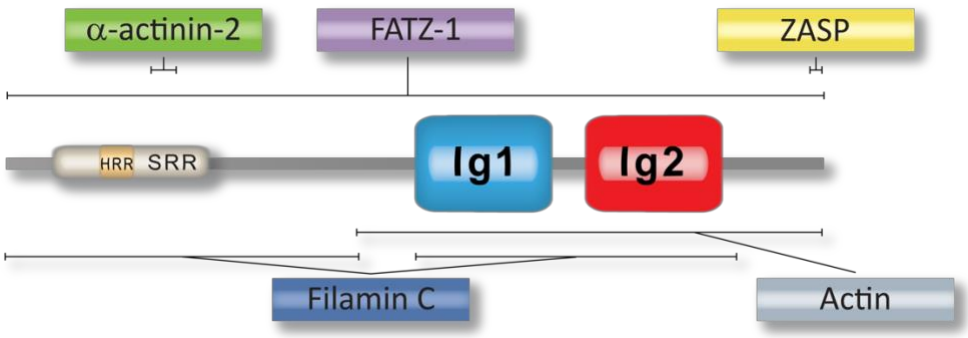

Figure 3. The myotilin interactome, courtesy of the Djinovic lab.

Myotilin interacts with several major Z-disc proteins. The interaction with α-actinin is established through the serine rich region, with ZASP at the C-terminal region and with actin through the C-terminal half of the protein. Myotilin also interacts with FATZ and filamin-C, but the exact binding region is not known.

The full-length myotilin resembles α-actinin in the ability to cross-link F-actin as shown by co-sedimentation assays and using transmission electron microscopy (Salmikangas et al., 2003). However, it turns out that myotilin is a weaker F-actin cross-linker, as the F-actin bundles detected when myotilin was used were loose and curved compared to the thick, rigid bundles α-actinin creates (Salmikangas et al., 2003). The F-actin bundling property of myotilin is suggested to come from its ability to form dimers via its Ig domains (Salmikangas et al., 2003).

F-actin binding and bundling property seem to come from its C-terminal half. While the full-length protein is able to form bundles of F-actin, the N-terminal half is not able to do so. Finally, a truncated myotilin construct which lacks the first 184 residues was determined as the minimal necessary region for F-actin bundle formation (von Nandelstadh et al., 2005). Similarly, a construct containing amino acids 214-498 was shown to be sufficient for binding of myotilin to actin (von Nandelstadh et al., 2005). It is however worth noting that individual Ig-like domains can as well bind actin, however with lower affinity. The C-terminal and especially the N-terminal flanking regions of the Ig-like domains seem to increase the binding and play an important role in stabilizing the interaction with F-actin (von Nandelstadh et al., 2005), (Kostan et al., unpublished data). Interestingly, apart from its F-actin organizing function, myotilin was also reported to have a stabilizing effect on F-actin, as it impairs F-actin depolymerization by latrunculin A (Salmikangas et al., 2003).

Diseases associated with myotilin

Although it plays an important role in the muscle, knock-out of the myotilin gene does not cause any detrimental phenotype in mice, as both the structure and the function of the sarcomere are preserved (Moza et al., 2007). To offer an explanation, it was suggested that proteins related to myotilin, namely, paladin and myopalladin, might act to replace myotilin in its absence. However, mice lacking myotilin and expressing very small amounts of palladin were shown to exhibit a surprisingly mild phenotype (Moza et al., 2008).

In contrast, partial myotilin deletions (either of the N- or the C-terminal region) cause disarrangement of the sarcomere (Salmikangas et al., 2003; van der Ven et al., 2000). Similarly, mutations in the myotilin gene which affect its function were shown to be more harmful than complete deletion of the protein. Hence, point mutations, including K36E, S39F, S55F, S60C, Q74K and S95I, are responsible for a severe group of myofibrillar myopathies (MFM), named myotilinopathies, as well as a rare disease named Limb-gridle muscle dystrophy 1A (LGMD1A) caused by a T57I mutation in myotilin (Hauser et al., 2000; Selcen, 2008; Selcen and Engel, 2004). Patients carrying these mutations exhibit common characteristics of all myotilinopathies, including Z-disc streaming, muscle weakness and myofibrillar degeneration, but also some more specific ones like recognizable dysarthric pattern of speech in the case of LGMD1A (Hauser et al., 2000). A similar phenotype was observed in mice bearing the T57I mutation, where large aggregates of mutated myotilin alongside other Z-disc proteins including α-actinin, filamin-C and titin were formed (Garvey et al., 2006). Although located in the serine rich region known to interact with α-actinin, these mutations do not impair the myotilin-α-actinin interaction (Hauser et al., 2000).

Additionally, it is unlikely that these mutations affect F-actin binding, as myotilin constructs bearing four of these myopathy related mutation (S55F, T57I, S60C and S95I) showed no difference in binding to F-actin compared to the wild type (von Nandelstadh et al., 2005). Impaired degradation of mutated myotilin might ,however, play a role in developing myopathies, as recombinant myotilin carrying either S55F, T57I or S60C mutations was degraded at a slower rate than the wild-type protein (von Nandelstadh et al., 2011).

Indications of calcium-dependent regulation of myotilin

Apart from its role in F-actin binding and crosslinking which contribute to the overall organization of the sarcomere, not much is known about the function of myotilin in the Z-disc. In the more recent years, attempts have been made to gather information on myotilin regulation. Consequently, it was shown that myotilin is cleaved by calpain, a key protease of the muscle (von Nandelstadh et al., 2011). Results of another study suggest that MURF-1, a muscle specific E3-ligase of the ubiquitin-proteasome related protein degradation pathway, might be involved in myotilin degradation (Witt et al., 2005). Interestingly, both calpain and MURF-1 are activated in processes related to calcium signaling. Additionally, the more dynamic nature of myotilin was recently brought to life in context on muscle repair and remodeling. Myotilin was enriched in muscle lesions related to delayed onset muscle soreness and eccentric exercise and was proposed to be a marker of myofibrillar remodeling (Carlsson et al., 2007), yet another process which heavily relies on calcium signaling. In light of these findings, we pursued to find a concrete link between the Ca driven signaling and myotilin. Before the aim of the thesis is stated, the following chapter provides the reader with a deeper understanding of the importance of Ca^{2+}-dependent signaling in the striated muscle and Calcineurin, a major mediator of the Ca^{2+} signal transduction.

Part II: Introduction to Calcium signaling in striated muscle and Calcineurin, its key mediator

Calcium is an essential second messenger

Calcium (Ca^{2+}) is the most abundant metal and the fifth most common element in the human body, after hydrogen, oxygen, carbon and nitrogen. As such, calcium is an essential component of life. While the majority of this metal is bound in form of salts in the skeletal system, less then 1% of Ca^{2+} resides free, and is mostly found in the extracellular fluid (Beto, 2015). A great portion of the cell's energy is invested in keeping Ca^{2+} outside of the cytosol, resulting in a 20,000-fold gradient of Ca^{2+} being maintained between the intracellular (around 100 nM) and the extracellular (2-4 mM) environment. At first, this was necessary for survival, as Ca^{2+} is known to be toxic in high amounts due to its ability to bind and precipitate phosphate (Clapham, 2007). However, what was once a rigorously controlled fight for survival, became, in the course of evolution, a valuable tool as organisms utilized the difference and change in Ca^{2+} concentration to communicate with each other and respond to their ever-changing environment. From a potentially detrimental component, Ca^{2+} became the key regulator of a vast range of physiological processes (Berridge et al., 2000).

Subtle changes in Ca^{2+} concentrations are used to transmit information and provoke an appropriate reaction: starting from a common set of Ca^{2+} receptors and sensors, elaborate and specialized signal transduction pathways have evolved to use Ca^{2+} as a secondary messenger and

target complex processes like activation of an adaptive immune response or mediate signal transmission in a neural network (Bootman, 2012). Muscle contraction, however, is maybe the best-known example of a process in which Ca^{2+} plays an essential role. Both muscle types, namely smooth muscles responsible for internal organ movement, and striated muscles, which allow heart contraction and voluntary motion, depend on Ca^{2+} to function. The principle of contraction is the same in the two muscle types: an increase in the cytosolic Ca^{2+} levels stimulates the contractile apparatus built out of two main proteins, actin and myosin (Kuo and Ehrlich, 2015).

Contraction in striated muscle

Contraction is especially efficient in striated muscles (Figure 4). By contrast to smooth muscles which use secondary messengers to sense Ca^{2+}, striated muscles are tightly coupled to motoneurons resulting in a rapid Ca^{2+} and voltage-dependent signal transduction. Additionally, the unique structure of striated muscles makes the information transmission efficient; they are highly coordinated due to their organized networks of repeating contractile units, sarcomeres (Kuo and Ehrlich, 2015).

In striated muscles, binding of a neurotransmitter, such as acetylcholine, to the cell surface triggers membrane depolarization and opening on voltage-gated channels. Intracellular Ca^{2+} concentration increases as Ca^{2+} is release from a specialized Ca^{2+} containing intracellular compartment, the sarcoplasmic reticulum. Ca^{2+} binding to troponin in the tropomyosin complex induces a conformational change, and tropomyosin, which is wrapped around actin filaments, moves to reveal a myosin binding site on actin. Subsequently, myosin binds actin, which causes a release of a myosin bound ADP, generating energy that powers contraction. Finally, binding of an ATP molecule to myosin results in muscle relaxation as myosin hydrolyses ATP and disassociates from actin to allow for the next contraction cycle to occur (Gehlert et al., 2015; Kuo and Ehrlich, 2015).

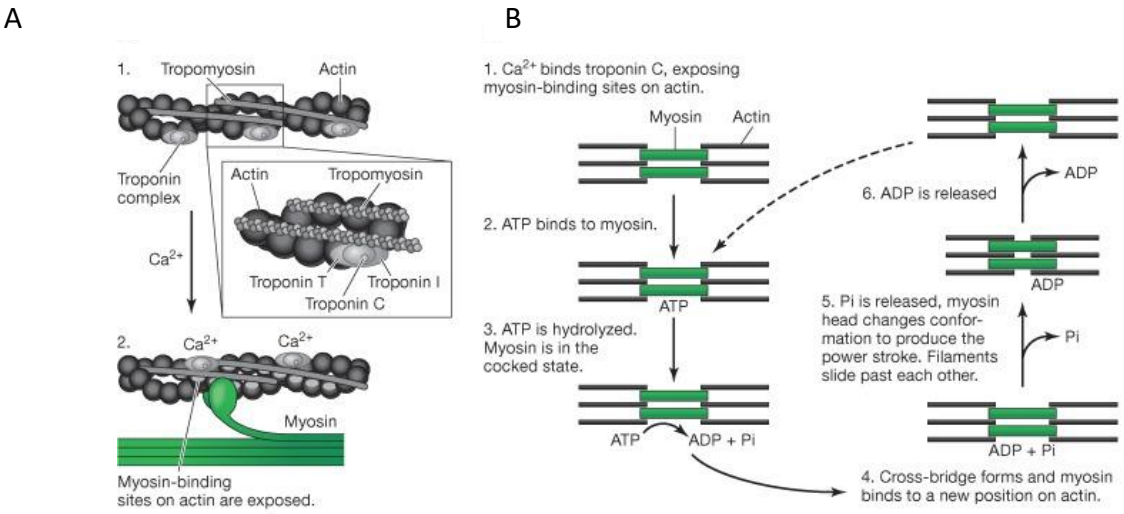

Figure 4. Steps of the contraction process, taken from Kuo and Ehrlich, 2015.

(A) Representation of the actomyosin contractive apparature. The tropomyosin complex is wraped around filamentous actin composed out of actin monomers. The troponin complex composed out of troponin T, troponin C and troponin I interacts with actin and tropomyosin and keeps the myotilin binding site unaccessible. When Ca^{2+} levels increase, Ca^{2+} binds troponin C and a myosin binding site gets exposed on actin as a result of conformational change. (B) Flowchart of the most important spets of

contraction. Myosin which has hydrolysed ATP to ADP and Pi binds actin. Release of Pi results in a conformational change of the myosin head and a power stroke which generates contraction. Myosin dissasociates from actin upon releasing ADP and binding a new ATP molecule.

Calcium signaling in the striated muscle

While the general increase in Ca^{2+} concentration drives contraction, striated muscles can sense subtle differences in the strength, duration, and spatial distribution of the Ca^{2+} signal. Hence, certain excitation patterns, which determine the frequency and amplitude of Ca^{2+} pulses, selectively activate specialized activates Ca^{2+}-dependent enzymes, Ca^{2+} decoders. Ca^{2+} decoders set in motion downstream signal transduction modulate the physiology and the phenotype of the striated muscle (Tavi and Westerblad, 2011). The ability of the muscle cell to recognize and distinguish different spatiotemporal Ca^{2+} patterns is essential for reacting to constantly changing requirements, which dictate muscle development and differentiation, maintenance and homeostasis, hypertrophy and remodeling, as well as atrophy and protein degradation (Hudson and Price, 2013; Tallis et al., 2018; Tu et al., 2016).

Muscle differentiation and fiber-type switching are one of the key Ca^{2+} driven processes. Depending on the Ca^{2+} signal, striated muscles exhibit two main fiber types: while sporadic, but powerful strokes of Ca^{2+} are characteristic for the fast-twitch muscle type, continuous Ca^{2+} pulses of low amplitude promote the slow-twitch muscle type (Schiaffino and Reggiani, 2011; Tavi and Westerblad, 2011). The two types differ in the energy source and metabolism they use, their endurance and their operational protein repertoire. Fast-twitch muscles fatigue easily as they utilize carbohydrates to generate powerful, but short-lived bursts of energy. On the other hand, slow-twitch muscles are rich in mitochondria and utilize oxidative pathways to catabolize both carbohydrates and fats, leading to their high endurance (Olson and Williams, 2000; Schiaffino and Reggiani, 2011).

Calcineurin is a major Ca^{2+}-dependent phosphatase

One of the essential Ca^{2+} decoders is calcineurin (CN), a Ca^{2+} and calmodulin (CaM)-dependent phosphatase. Also known as PP2B, CN belongs to a family of serine/threonine (Ser/Thru) phosphatase along with protein phosphatase 1 (PP1), 2A (PP2A) and 2C (PP2C). CN is unique, as it is the only Ca^{2+}-dependent Ser/Thr phosphatase. Although ubiquitously produced in all human tissues, CN is most abundant in the nervous and the muscular system, where its concentration is measured to be 10-fold higher than in any other tissue (Aramburu et al., 2000).

The significance of CN as a Ca^{2+} decoder was first brought to attention when it was discovered that CN dephosphorylates and promotes nuclear translocation of the nuclear factor of activated T-cells (NFAT), a transcription factor which regulates gene expression to enable differentiation and proliferation of T cells and activate adaptive immune system (Shaw et al., 1995). Soon after, CN was associated with all three major Ca^{2+}-dependent systems: the nervous, the muscular and the immune system.

Calcineurin regulates major processes in striated muscles

It was not surprising to assume that CN could be involved in muscle regulation, as it was known that NFAT also played a role in muscle, where it induces muscle specific gene expression (Boss et al., 1998). Additionally, the use of ground-breaking immunosuppressant drugs cyclosporin A (CsA) and FK-506, that prevent organ rejection in transplant patients by specifically inhibiting CN mediated T cell activation, lead to muscle mass reduction and wasting (Goy et al., 1989). Today, CN is recognized as the vital mediator of muscle differentiation and striated muscle type switching. Through its elaborate network of interconnecting pathways, CN controls and balances key process like muscle hypertrophy, protein degradation and muscle regeneration to bring about remodeling of the fast-twitch muscle fibers, which gives rise to the slow-twitch phenotype (Hudson and Price, 2013; Shimizu et al., 2017; Tu et al., 2016). The role CN has on promoting long term shifts in gene expression needed to initiate muscle differentiation and fiber-type transformation is best understood of all of these functions (Bassel-Duby and Olson, 2006; Hudson and Price, 2013; Olson and Williams, 2000; Schiaffino and Reggiani, 2011).

In a developing muscle, CN drives specific skeletal muscle cell differentiation by upregulating expression of myogenic genes and regulating key transcription factors such as NFAT, MEF2, myogenin and MyoD (Delling et al., 2000; Friday et al., 2003). As already mentioned, although preset gene expression programs drive differentiation of a specific muscle fiber type prior to innervation, a crucial property of the muscle is that it remains adaptive to changing neural stimuli. CN, along with other Ca^{2+} decoders, acts as a nodal point to mediate the intimate interplay between neural signaling and expression of adequate muscle genes. In a formed muscle, CN again plays a pivotal role by promoting muscle growth and tissue specialization upon chronic muscle overload, by driving transition from the slow to the fast muscle fiber (Chin et al., 1998; Schiaffino and Reggiani, 2011). The same transcription factors used in development, including NFAT and MEF2, are now recruited to synergistically promote gene expression reprograming (Friday et al., 2003; Swoap et al., 2000). This is primarily achieved by activating genes responsible for mitochondrial biosynthesis and transcription of a specific set of muscle genes, which results in a major turnover of many muscles proteins, like myosin, troponin and myoglobin, as the fast-twitch fiber specific isoforms are being replaced by their slow-twitch fiber counterparts (Olson and Williams, 2000).

As the key sensor of Ca^{2+} dynamics, CN is also activated during muscle regeneration. It is expressed in proliferating satellite cells (muscle stem cells), which undergo differentiation and fuse with existing skeletal muscle cells to enable repair of the injured tissue (Sakuma et al., 2003; Tu and Borodinsky, 2014; Tu et al., 2016). This was shown by either expressing a constitutively active form of CN to enhance regeneration or by inactivating CN using specific inhibitors like CsA, which resulted in muscle atrophy in rodents (Sakuma et al., 2003; Stupka et al., 2007). Additionally, a constitutively active CN isoform (CNAβ1) was shown to enhance rebuilding of the damaged muscle tissue in mice by suppressing FoxO, a transcription factor responsible for transcription of the muscle specific E3 ligase, MuRF1 (Lara-Pezzi et al., 2007). More recent, however, a study has been published suggesting that CN promotes protein degradation by dephosphorylating and activating FoxO, which results in enhanced MuRF1 expression and higher degree of muscle protein degradation in Zebrafish cardiomyocytes (Shimizu et al., 2017).

Structure and activation of calcineurin

CN is a heterodimer formed through tight association of a 59 kDa catalytic subunit A (CNA) and a 19 kDa regulatory subunit B (CNB) (Figure 5A). Three isoforms of catalytic subunit A (CNA-α, CNA-β and CNA-γ) are encoded by three separate, highly conserved genes. CNA-β is the most ubiquitous isoform, as opposed to the more tissue specific CNA-α and CNA-γ expressed in neurons and testes respectively. CNA consists of four distinct sections: the catalytic domain which contains the active center, the CNB binding region, the largely disordered CaM binding segment and the autoinhibitory peptide (Rusnak and Mertz, 2000). The active center of CN requires binding of two metals, namely Fe^{3+} and Zn^{2+}, to function. In the active center Asp90, His92, Asp188, a water molecule, a phosphate oxygen, and Asp118, Asp150, His199 and His281 coordinate Fe^{3+} and Zn^{2+} respectively (Griffith et al., 1995; Rusnak and Mertz, 2000). Although Fe^{3+} and Zn^{2+} are most commonly found in the active center residues, it has been shown that CN can also be activated in presence of divalent metals such as Mn^{2+}, Ni^{2+}, Co^{2+} and Mg^{2+} (King and Huang, 1984).

Two different genes encode the regulatory subunit B: CNB-α which is the predominant form, and CNB-β which can solely be isolated from testes. CNB is composed out of four EF-hand motifs, each of which can facilitate binding of one Ca^{2+} ion. The individual EF-hand motifs bind Ca^{2+} with different affinities. The two C-terminally located motifs bind Ca^{2+} with high affinity (K_D in the nM range) and are thought to have a structural role in stabilizing the CN fold. The remaining two sites are weaker Ca^{2+} binders (K_D in the μM range) and act as Ca^{2+} sensors to regulate CN activity (Li et al., 2011; Rusnak and Mertz, 2000). Interestingly, the N-terminal end of the CNB can be myristoylated. Although it was speculated that this modification might affect substrate binding, activity or membrane anchoring, apart from the myristoylated CN exhibiting higher thermal stability, there seems to be no difference between the myristoylated and the non-myristoylated version of the phosphatase (Griffith et al., 1995; Rusnak and Mertz, 2000).

Ca^{2+} induced conformational changes result in CN activation (Figure 5B). Once muscle cells experience a sustained increase in Ca^{2+} levels, Ca^{2+} binds the two low affinity binding sites in the CNB triggering a conformational change which in turn leads to a release of the CaM binding domain and subsequent CaM binding (Yang and Klee, 2000). Additional structural changes follow that induce displacement of the autoinhibitory peptide from the active center resulting in full activation of CN (Li et al., 2011; Rumi-Masante et al., 2012).

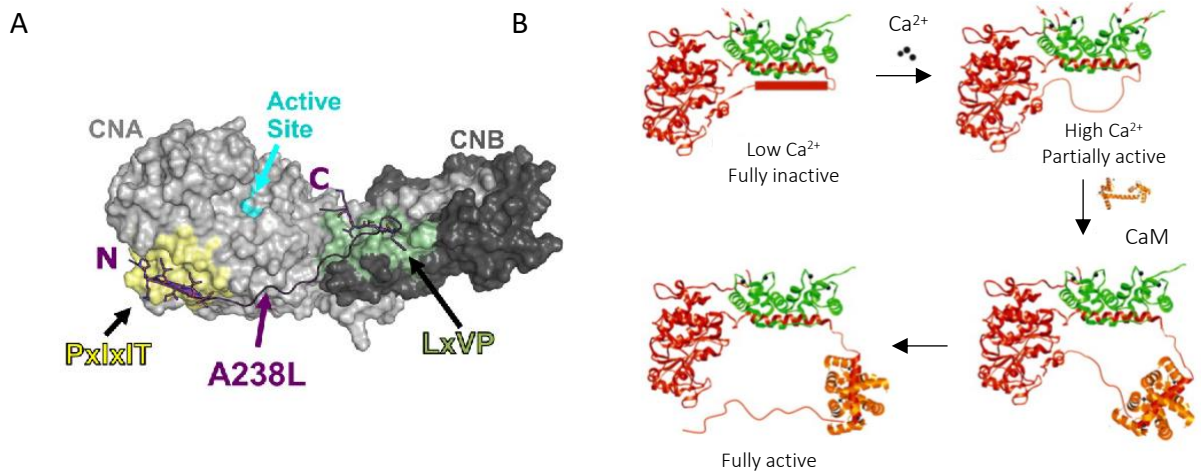

Figure 5. Calcineurin structure and activation, taken from (A) Pati et al., 2015. and (B) Li et al., 2011.

(A) Structure of CN in complex with a A238L peptide which contains both the PxIxIT and the LxVP motif taken from Pati et al., 2015. CN (surface representation) is a heterodimer which consists out of a catalytic subunit A (light gray) which contains the active center (cyan) and a regulatory subunit B (dark gray). The protein has two substrate binding interfaces: the first one on the subunit A which recognizes the PxIxIT motif (yellow) and the second one at the CNA-CNB interface which binds the LxVP motif (green). The A238L peptide (cartoon, purple) is a viral inhibitor of CN which contains both CN bindig motifs and is used to show how CN interacts with these motifs in this and other proteins which interact with CN. (B) Mode of CN activation taken from Li et al., 2011. At low Ca^{2+} levels, only the two high affinity Ca^{2+}-binding sites are occupied and the CaM binding domain stabilizes the interaction between the CN autoinhibitory region and the CNA. When the Ca^{2+} concentration increases, all Ca^{2+}-binding sites of CN are occupied. Additionally, CaM is activated and binds C which results in a conformational change and a dissociation of the autoinhibitory region from CNA, resulting in a fully active state of CN.

Calcineurin binding motifs

CN recognizes and binds its substrates via two distinct CN binding motifs (Li et al., 2011). The first discovered motif was the PxIxIT motif, a consensus motif found in all four NFAT isoforms which are known to bind CN (Aramburu et al., 1998). Upon further investigation of the NFAT-CN interaction, a second conserved binding motif, the LxVP motif, was identified (Park et al., 2000). Both motifs are short linear motifs, meaning that they are found in disordered regions of CN substrates (Sheftic et al., 2016). The two motifs interact with different parts of the CN heterodimer and do not compete for CN binding. The PxIxIT motif adopts a beta strand structure upon binding to a side of the CNA subunit and it thought to primarily stabilize the interaction and increase the affinity of binding (Li et al., 2004; Li et al., 2007). The LxVP motif, which remains extended, binds to a hydrophobic groove at the CNA-CNB interface (Grigoriu et al., 2013; Rodriguez et al., 2009). NFAT peptides containing either the PxIxIT or the LxVP motif can diminish CN activity. However, unlike the peptides carrying the PxIxIT motif, NFAT peptides which contain the LxVP motif were shown to compete with the standard CN substrate peptide (the RII peptide from the cAMP-dependent protein kinase type II-alpha regulatory subunit) and impair CN activity to activate NFAT *in vivo*. It was shown later that the peptides containing the LxVP motif bind the same CN interface as the well-established CN inhibitors CsA and FK506 (Griffith et al., 1995; Rodriguez et al., 2009). This was crucial for understanding the mechanism in which these inhibitors inactivate CN and for showing the importance of the LxVP motif. The LXVP motives were also reported to play a significant role in substrate dephosphorylation, as substrates with mutations in the LxVP were phosphorylated less than the wild-type substrates or those carrying mutations in the PxIxIT motif (Rodriguez et al., 2009). Although the number of identified CN substrates has grown over the years, big efforts are being made to extend the pool of CN substrates and especially gather knowledge on the poorly characterized LxVP bearing CN substrates.

Calcineurin associated diseases

Because it plays a fundamental role in regulating major Ca^{2+}-dependent processes, CN has been associated with multiple severe diseases. CN is targeted by pathogens to compromise the immune response of the host, but at the same time, defects in its function can contribute to development of autoimmune diseases (Azzi et al., 2013; Emal et al., 2019). Additionally, multiple neurodegenerative disorders including Parkinson's, Alzheimer's and Huntington's disease are thought to be connected to altered CN signaling (Caraveo et al., 2017; Pineda et al., 2009; Reese and Taglialatela, 2011).

CN also plays a prominent part in pathologies which effect the muscle tissue (Sakuma and Yamaguchi, 2010). While elevated CN activity was shown to be a causative factor of cardiac hypertrophy (Sussman et al., 1998), impaired function of this phosphatase which leads to the loss of muscle mass has been related to aging, sepsis, Cushing syndrome, obesity and diabetes type 2 (Tallis et al., 2018).

Part III: Calcineurin signaling in the Z-disc

It is essential that CN activity is controlled in a spatial and temporal manner to avoid any harmful effects an impaired Ca^{2+} signal transduction would have on the muscle. The Z-disc, which was first characterized as the key stabilizing component that links sarcomeres and organizes contraction, has been shown to act as a central signaling hub of striated muscles (Frank et al., 2006). The highly dynamic architecture of the Z-disc, defined by complex layers of protein interactions and hierarchy, serves as an interface at which coordination of major modes of muscle regulation, including Ca^{2+} and mechano-sensing, and post-translational modification, occurs. Despite this fact, our knowledge on the role of CN in the Z-disc is limited (Frank and Frey, 2011; Frank et al., 2006).

With the discovery of several Z-disc proteins that bind CN, it became evident that Z-disc acts both as an important CN regulator and as a platform for CN signaling. The best-known example for CN regulation in the Z-disc is the manner in which the interplay between CN and its inhibitor FATZ is determined by the two isoforms of α-actinin. As already mentioned, α-actinin is the core Z-disc protein which crosslinks F-actin and interacts with a number of other Z-disc proteins, including filamin C, ZASP, FATZ, myotilin and titin. Two different sarcomeric α-actinin isoforms exist, namely α-actinin-2 and α-actinin-3, and FATZ has been shown to predominantly bind α-actinin-2 over α-actinin-3 (Seto et al., 2013). Consequently, in fast-twitch muscles where α-actinin-3 is present, FATZ is free in the cytosol and interacts with CN to inhibits its activity (Frey et al., 2000). However, many individuals carry a stop codon polymorphism in the *ACTN3* gene and exhibit only partial α-actinin-3 expression or lack α-actinin-3 completely. In this case, FATZ binds preferentially α-actinin-2 over CN, and this lifts inhibition on CN, which can in turn be activated by a prolonged Ca^{2+} signal to trigger muscle type switching. Because of its ability to restrict muscle fiber remodeling and preserve the fast-twitch fiber phenotype, *ACTN3* is popularly known as the "gene of speed" that is believed to elevate muscle performance and distinguish elite athletes form the general population (Seto et al., 2013).

Although FATZ is the best-known CN binder in the Z-disc (Frey et al., 2000), several other proteins, including ZASP, MLP and myopodin, have been reported to interact with CN. Similar to FATZ, it was shown that ZASP interacts with CN, leading to decrease in CN activity (Lin et al., 2013). Neither ZASP nor FATZ have one of the two established PxIxIT or LxVP motifs and the molecular details of these interactions are yet to be established. On the other hand, myopodin was shown to be a substrate of CN. Myopodin is a unique Z-disc protein which bundles F-actin, but can also be transported into the nucleus under stress conditions, thus acting as a stress-sensor in the Z-disc. The nuclear translocation of myopodin depends on its phosphorylation status: it is inhibited when the protein is phosphorylated by protein kinase A (PKA) or calcium/calmodulin-dependent kinase (CaMKII), but becomes more prominent once its dephosphorylated by CN (Faul et al., 2007). Finally, the muscle LIM protein (MLP) was also reported to interact with CN. MLP is neither the

substrate nor the inhibitor of CN, this protein is essential for the CN signaling as it anchors CN in the Z-disc, enabling activation of the CN-NFAT signaling pathway at the sarcomere boarders (Heineke et al., 2010).

Part IV: Open question on the regulation and dynamics of myotilin

Apart from myotilin's role in F-actin binding and crosslinking, which contribute to the overall organization of the sarcomere, many questions regarding myotilin remain to be addressed. Most notably, there is a rising necessity of understanding myotilin dynamics and regulation in context of Ca^{2+} mediated signal pathways and phosphorylation.

Although progress was made to characterize the interaction of myotilin with F-actin, it is not fully understood how myotilin interacts with its other binding partners. It is common for Z-disc proteins to contain one or more disordered stretches, which makes it challenging to narrow down regions of interaction between isolated Z-disc proteins *in vitro*. Hence, apart from confirming the interaction, no detailed mapping of the myotilin's interaction with FATZ or filamin-C has been achieved so far. In contrast, due to extensive knowledge on PDZ domains and the ways they interact with their binding partners, more is known about the interaction of myotilin with ZASP. In a typical manner, the PDZ domain of ZASP interact with the C-terminal residues of myotilin (Lee and Zheng, 2010; von Nandelstadh et al., 2009). However, the interaction of the PDZ domain of ZASP with myotilin provided the myotilin community with a unique insight into the complexity and regulation of this interaction: binding of myotilin to this PDZ domain is promoted once the C-terminal end of myotilin is phosphorylated by a Ca^{2+} sensitive protein kinase CaMKII (von Nandelstadh et al., 2009). In addition, a recent study, where mass spectroscopy of the whole Z-disc was performed, proposed that the Z-disc is a hot-spot of regulation, as many of its component were identified to be phosphorylated. On this occasion, two Ser residues of myotilin, Ser 229 and Ser233 were reported to be phosphorylated (Reimann et al., 2017). Notably, these residues reside in the region speculated to be of importance for F-actin binding and bundling (von Nandelstadh et al., 2005), (Kostan, unpublished data). Together, these two findings rise an interesting question about the potential regulation of other interactions from the myotilin interactome via post-translational modification, particularly phosphorylation.

Attempts have also been made to gather information on myotilin turnover. Consequently, it was shown that calpain, a key protease of the muscle cleaves myotilin *in vitro* (von Nandelstadh et al., 2011). Two cleavage events of myotilin were observed, the seldom cleavage at the site $^{254}I/Q^{255}$, and the frequent cleavage at the site $^{225}S/Q^{226}$ of myotilin. This seems to be an important mechanism of regulating myotilin stability and homeostasis, as the cleavage was less efficient in case of myotilin constructs which carried mutations associated with MFM (von Nandelstadh et al., 2011). In addition to being cleaved by calpain, myotilin is a potential substrate of muscle RING-finger protein-1 (MURF-1) also known as TRIM63, a muscle specific E3-ligase of the ubiquitin-proteasome related protein degradation pathway (Witt et al., 2005). Interestingly, both calpain and MURF-1 are activated in processes related to calcium signaling; while calpain activation depends on Ca^{2+} binding (Dayton et al., 1976), MURF-1 expression is upregulated in presence of Ca^{2+} in a CN-dependent manner by the CN-FoxO signaling axis (Shimizu et al., 2017).

Furthermore, there is a fundamental lack of knowledge on myotilin dynamics in the muscle filed. The role of myotilin in the muscle development remains unclear. On the one hand, together with other Z-disc proteins (α-actinin, ZASP, etc.) myotilin was reported to be one of the components of Z-bodies (Wang et al., 2011) which act as nuclei around which the Z-disc is organized and built during myogenesis. On the other hand, significant expression of myotilin has only been detected in later stages of muscle differentiation, once the Z-disc core has already been assembled. Moreover, premature expression of myotilin in early stages of muscle development, led to problems in proper sarcomere assembly due to strong F-actin bundling caused by myotilin (Salmikangas et al., 2003).

Myotilin has also been investigated in the context of muscle repair and remodeling. Myotilin enrichment was observed using immunofluorescence in muscle lesions related to delayed onset muscle soreness (DOMS) and eccentric exercise in muscle tissue samples extracted from a pool of 16 male subjects. DOMS results from overstretching of myofibers and is followed by formation of new sarcomeres. Since specific enrichment of myotilin, but not α-actinin or desmin, was detected in lesions containing F-actin, it was suggested that myotilin acts as recruiter of monomeric G-actin in initial stages of muscle remodeling, when other Z-disc proteins are absent. As such, myotilin could be used as a prominent marker of muscle remodeling associated to DOMS and eccentric exercise (Carlsson et al., 2007). Muscle repair and remodeling is yet another process which heavily relies on calcium signaling and it is also regulated by CN.

Aim of the study

In light of the aforementioned findings, it seems that myotilin regulation as well as its dynamics are driven by Ca^{2+} associated enzymes and processes, some of which are dependent on CN signaling. Nevertheless, a clear link between CN and myotilin is yet to be discovered. So far, myotilin has been speculated to be either directly or indirectly involved in the elaborate CN signaling network, solely due to the fact that CN and myotilin share a common binding partner, FATZ (Gontier et al., 2005). Therefore, in this thesis we (I) will employ an integrative approach by combining specific biochemical, biophysical and structural methods to answer three main questions:

1) Does myotilin directly interact with CN? To address this question, we will performed two sets of pulldown experiments: one with immobilized Strep-tagged myotilin and the other with immobilized His-tagged CN. To specify the exact region of myotilin responsible for CN binding, a CelluSpots peptide array assay will be used.

2) How does myotilin interact with CN? Here we will try to characterize interaction of myotilin with CN, either by SEC-MALS, focusing on stability and the stoichiometry of the complex, or by ITC used to determine the dissociation constant and determine the contribution of changes in enthalpy and entropy to the final free energy of binding. Finally, we used X-ray crystallography to enlighten the molecular principles which drive this interaction.

3) Is myotilin a substrate of CN? For this, phosphorylated peptide of myotilin would be tested in CN based dephosphorylation assays. Phosphorylated residues will be selected based on prior knowledge from the literature.

Materials and Methods

Buffers, stocks and media

50x Tris-acetic-EDTA (TAE) buffer
2 M mM Tris, 1 M glacial acetic acid, 50 mM EDTA pH 8.0

Lysogeny broth (LB) agar
10 g tryptone, 5 g yeast extract, 10 g NaCl, 14 g agar, 1 l with ddH_2O

Antibiotic Stocks
1000x carbenicillin: 100 mg/ml, dissolved in ddH_2O, filtered through 0.45 μm pore filter
1000x chloramphenicol: 34 mg/ml, dissolved in 100% ethanol

Protease inhibitor cocktail
100 μM bestatin hydrochloride, 14 μM E64 protease inhibitor, 10 μM Pepstatin A, 1 μM phosphoramidon disodium salt, dissolved in DMSO

Media
LB media:
10 g tryptone, 5 g yeast extract, 10 g NaCl, 1 l with ddH_2O

ZYP-5052 auto-induction media:
ZY: 10 g casein, 5 g yeast extract, 1 l ddH_2O)
20xP: 0.5 M $(NH_4)_2SO_4$, 1 M KH_2PO_4, 1 M Na_2HPO_4
50x5052: 0.5% (v/v) glycerol, 0.05% (w/v) glucose 0.2% (w/v) alpha-lactose
500x $MgSO_4$: 1 M $MgSO_4$

Terrific Broth (TB) media:
Solution A (for 900ml): 12 g tryptone, 24 g yeast extract, 4 ml glycerol
Solution B (for 100ml): 2.31 g KH_2PO_4, 12.54 g K_2HPO_4, pH 7.2

Myotilin Purification
Myotilin Lysis Buffer (Buffer M1): 50 mM Tris, 150 mM NaCl, 5% glycerol, 2 M urea, 0.5% Triton X-100, 0.2 mM EDTA, 20 mM imidazole, pH 8.0
Myotilin His Buffer A (Buffer M2): 50 mM Tris, 150 mM NaCl, 5% glycerol, 2 mM β-mercaptoethanol, pH 7.5
Myotilin His Buffer B (Buffer M3): 50 mM Tris, 150 mM NaCl, 0,5 mM NaCl, 5% glycerol, 2 mM β-mercaptoethanol, pH 7.5
Myotilin 3C Cleavage Dialysis Buffer (Buffer M4): 50 mM Tris, 150 mM NaCl, 1 mM DTT, 5% glycerol, pH 7.5
Myotilin Resource S Buffer A (Buffer M5): 20 mM Hepes, 5% glycerol, pH 7.0
Myotilin Resource S Buffer B (Buffer M6): 10 mM Hepes, 1 M NaCl, 5% glycerol, pH 7.0
Myotilin SEC Buffer (Buffer M7): 20 mM Tris, 150 mM NaCl, 5% glycerol, pH 7.5

Calcineurin Purification

Calcineurin Lysis Buffer (Buffer C1): 50 mM Tris, 500 mM NaCl, 5 mM imidazole, EDTA free protein inhibitor cocktail, 0.5 mM PMSF, pH 8.0
Calcineurin His Buffer A (Buffer C2): 50 mM Tris, 500 mM NaCl, pH 8.0
Calcineurin His Buffer B (Buffer C3): 50 mM Tris, 500 mM NaCl, 500 mM Imidazole, 0.5 mM PMSF, pH 8.0
Calcineurin Dialysis Buffer (Buffer C4): 20 mM Tris, 100 mM NaCl, pH 8.0
Calcineurin Resource Q Buffer A (Buffer C5): 50 mM Tris, 0.5 mM $CaCl_2$, 1 mM EDTA, 0.5 mM PMSF, pH 8.0
Calcineurin Resource Q Buffer B (Buffer C6): 50 mM Tris, 1M NaCl, 0.5 mM $CaCl_2$, 1 mM EDTA, 0.5 mM PMSF, pH 8.0
Calcineurin SEC Buffer (Buffer C7): 20 mM Tris, 150 mM NaCl, 0.5 mM TCEP, 1mM $CaCl_2$, 0.5 mM PMSF, pH 7.5

CelluSpot Assay

TBS Buffer: 20 mM Tris, 100 mM NaCl, pH 7.5
TBST Buffer: 20 mM Tris, 100 mM NaCl, 0.05% Triton X-100, pH 7.5
Blocking solution: 2% BSA (w/v), dissolved in TBS Buffer

SLS Buffer

20 mM Hepes, 100 mM NaCl, pH 7.5

PullDown Assay

PullDown Equilibration Buffer (Buffer PD1): 20 mM Hepes, 100 mM NaCl, 2.5 % glycerol, pH 7.5
PullDown Elution Buffer (Buffer PD2): 50 mM Tris, 0.5 M NaCl, 0.5 M imidazole, 7 M urea, pH 8.0

ITC Buffer

20 mM Hepes, 150 mM NaCl, 1 mM $CaCl_2$, pH 7.5

5x Calcineurin Activity Buffer

50 mM Tris, 100 mM NaCl, 0.5 mM $CaCl_2$, 0.5 mM DTT, 5 mM $MgCl_2$, pH 7.5

10x AKT Activity Buffer

20 mM Tris, 100 mM NaCl, 10 mM $MgCl_2$, 10 mM ATP, pH 7.5

Peptide sequences

Peptide	Source	Purity	Description	Sequence
$Myot^{213-232}$	ProteoGenix	90.48%	Myotilin 213-232	HNSEHARLQVPTSQVRSRST
$Myot^{pSer229}$	ProteoGenix	98.76%	Myotilin 216-236, pSer229	EHARLQVPTSQVR(pSer)RSTSRGD
$Myot^{pSer231}$	ProteoGenix	97.34%	Myotilin 216-236, pSer231	EHARLQVPTSQVRSR(pSer)TSRGD
$Myot^{pSer233}$	ProteoGenix	96.95%	Myotilin 216-236, pSer233	EHARLQVPTSQVRSRST(pSer)RGD
RII	Coss lab-IMP	95%	PRKAR2A* 81-99	DLDVPIPGRFDRRV(pSer)VAAE

Table 1. Table of commercially synthetized peptides.
*cAMP-dependent protein kinase type II-alpha regulatory subunit

Plasmids and constructs

A truncated Calcineurin A: 1-391/B: 1-170 (N-His) construct encoded in the pET15b-derived p11 bicistronic vector was used throughout the duration of the entire project. This construct has a deleted C-terminal end of the subunit A, thus lacking the autoinhibitory and the calmodulin binding domain. An existing pETM20 plasmid encoding Myot$^{185\text{-}498}$ was modified for the purposes of this study. The C-terminal end of the construct was deleted to create a more stable Myot$^{185\text{-}444}$ (N-construct and this newly obtained plasmid was used as a template to introduce mutations either in the calcineurin binding motif or the putative phosphorylated serine residues. Summary of different constructs can be found in Table 2.

Name	Description/ Mutations	Affinity tags	Plasmid, resistance	Expression system, expression media
CN	A: 1-391/B: 1-170 wild-type	N-His6 /	pET15b-derived p11 ampicillin, tetracycline, chloramphenicol	*E. coli*, BL21(DE3) - RIL strain, TB media,
Myot$^{185\text{-}498}$	residues 185-489 wild-type	N-Trx-His6 C-Strep	pETM20 ampicillin	*E. coli*, C41 strain, ZYP-5052
Myot$^{185\text{-}444}$	residues 185-444 wild-type	N-Trx-His6 /	pETM20 ampicillin	*E. coli*, C41 strain, ZYP-5052
Myot$^{185\text{-}444}$ V222A P223A	residues 185-444 V222A, P223A	N-Trx-His6 /	pETM20 ampicillin	*E. coli*, C41 strain, ZYP-5052
Myot$^{185\text{-}444}$ R219Y Q221A	residues 185-444 R219Y, Q221A	N-Trx-His6 /	pETM20 ampicillin	*E. coli*, C41 strain, ZYP-5052
Myot$^{185\text{-}444}$ S229D	residues 185-444 S229D	N-Trx-His6 /	pETM20 ampicillin	*E. coli*, C41 strain, ZYP-5052
Myot$^{185\text{-}444}$ S229D S233D	residues 185-444 S229D, S233D	N-Trx-His6 /	pETM20 ampicillin	*E. coli*, C41 strain, ZYP-5052
Myot$^{185\text{-}444}$ S233D	residues 185-444 S233D	N-Trx-His6 /	pETM20 ampicillin	*E. coli*, C41 strain, ZYP-5052

Table 2. Table of protein constructs used or created for this study.

Cloning of myotilin constructs

A pETM20 plasmid encoding Myot$^{185\text{-}498}$ was used to delete the C-terminal end of the coding sequence and create a pETM20 plasmid encoding the Myot$^{185\text{-}444}$ construct. This newly created plasmid was used as template to introduce point mutations in the sequence encoding Myot$^{185\text{-}444}$ and produce all other constructs listed in Table 2.

To setup 50 µl of the polymerase chain reaction (PCR), 10-20 ng template DNA, 1 µM of both forward and reverse primer, 23 µl ddH2O and 25 µl 2x Phusion High Fidelity Master Mix (Thermo Scientific) were combined. The reaction was carried out using the program shown in Table 3.

Step	Temperature (°)	Time	Number of cycles
Initial denaturation	98	1 min	1
Denaturation	98	30 sec	
Annealing	72	5 sec	30
Elongation	72	2 min 50 sec	
Final Elongation	72	4 min	1
Hold	4	∞	1

Table 3. Typical PCR program used for cloning.

To check whether amplification took place, 5 µl of the PCR product were analyzed on a 1% agarose gel, and the remaining 45 µl were purified using the Gene JET PCR Purification Kit (Thermo Scientific). To digest the parental DNA, PCR product was incubated with 10 U DpnI (Thermo Scientific) in presence of 1x Tango Buffer (Thermo Scientific) at 37 °C for 1h.

After another purification step with Gene JET PCR Purification Kit (Thermo Scientific), amplified DNA was incubated with 10 U T4 Polynucleotide Kinase (Thermo Scientific) in ligase buffer at 37 °C for 40 min. Following ligation at RT for 1h in presence of 5 U T4 ligase (Thermo Scientific), 5 µl of the reaction were transformed into DH5alpha competent cells using the heat shock method. Cells were grown on agar plates supplemented with antibiotics at 37 °C overnight. Single colonies were selected, and isolated DNA was sent to Eurofins Genomics to confirm the sequence of the newly produced construct.

Expression and purification of myotilin

This protocol was used to express and purify all myotilin constructs and was kindly provided by Claudia Schreiner. A list of all buffers and media can be found in the Buffer, stocks and media section.

A pETM20 plasmid encoding the myotilin construct of interest was transformed into C41 competent cells using the heat shock method and grown on agar plates containing carbenicillin. Cells from the plate were used to grow at 37 °C and bacteria in LB medium supplemented with antibiotics overnight. Next, the overnight culture was used to inoculate ZYP-5052 media supplemented with antibiotics. The media was divided so that no more than 500 ml of bacterial solution was grown in one 2 l flask at 37 °C for 16 h. Cells were harvested at 4 °C and 6000 rpm for 15 min in a HITACHI Centrifuge using the R9A2 rotor.

Cells containing myotilin were resuspended with Buffer M1 supplemented with the Protease inhibitor cocktail and 0.5 mM PMSF, homogenized, sonicated (3x 3 min, 50% amplitude) and centrifuged at 4 °C and 20000 rpm for 25min in a HITACHI Centrifuge using the R20A2 rotor. Supernatant was applied onto two connected 5 ml HiTrap columns (GE Healthcare) pre-equilibrated with 8 CV of Buffer M2. After washing the columns with 4 CV of 4% His Buffer M3, myotilin was eluted at 100% Buffer M3. Myotilin was next cleaved overnight with the 3C protease (1:1000, w/w) while dyalized against Buffer M4. After a second HisTrap procedure, performed to

separate the cleaved from the uncleaved fraction, the flow-through was diluted 10 times with Buffer M5 and applied onto a cation exchange Resource S column (GE Healthcare) for further purification. Upon washing the column with 5 CV of Buffer M5, 10% of Buffer M6 was applied in a gradient spet over 5 CV. Myotilin was eluted with 25 CV using a gradient between 10 and 40% of Buffer M6. Finally, the myotilin peak was pooled, concentrated and applied onto a size exclusion HiLoad 26/60 S75 column (GE Healthcare) and eluted using a 1.2 CV isocratic gradient of Buffer M7.

Expression and purification of calcineurin

The protocol used for calcineurin expression and purification was adapted from a protocol kindly provided by Antonio Sponga. A plasmid containing the calcineurin construct was transformed into BL21 Codon Plus (DE3)-RIL competent cells using the heat shock method and grown on carbenicillin and chloramphenicol containing agar plates at 37 °C overnight. To make glycerol stocks, colonies from the plate were used to inoculate 10 ml LB media supplemented with antibiotics. Cells were harvested at 4 °C and 4000 rpm for 15 min, resuspended in 1 ml 20% glycerol and frozen. The glycerol stock was used to prepare overnight cultures for all expression experiments. Large scale expression was performed in TB media as followed: 1 l of media was combined with 3.3 ml of culture together with appropriate antibiotics and 250 ml of this solution was added to each of the 2 l flasks. Bacteria were grown at 37 °C until OD_{600} of 0.6 was reached, kept at 4 °C for 45 min and finally induced with 1 mM IPTG and incubated at 20 °C for 18 h. Harvesting was performed at 4 °C and 6000 rpm for 15min in a HITACHI Centrifuge using the R9A2 rotor.

Cells containing calcineurin were resuspended in Buffer C1 supplemented with the Protease inhibitor cocktail mix and DNaseI (1 mg/ml), homogenized and passed through cell disrupter (1.35 kbar) to release the protein. After addition of 0.5 mM PMSF, the solution was centrifuged at at 4 °C and 20000 rpm for 25min in a HITACHI Centrifuge using the R20A2 rotor. Resulting supernatant was applied onto a Talon column (GE Healthcare) pre-equilibrated with 5 CV of Buffer C2. After washing the column with 8 CV of Buffer C2, the protein of interest was eluted with 5CV of 100% Buffer C3. The eluate was diluted 2 times with Buffer C4 and dialyzed against Buffer C4 for 1.5 h. After additionally dilution the protein mixture 5 times with Buffer C5, the sample was applied onto an anion exchange Resource Q column (GE Healthcare). The column was washed over a series of steps using Buffer C5 and calcineurin was eluted with a gradient between 20% and 30% of Buffer C6. In the last step, calcineurin was purified using a HiLoad 26/60 S200 column (GE Healthcare) and eluted over a 1.2 CV isocratic gradient of Calcineurin SEC Buffer.

Dynamic Light Scattering (DLS)

DLS was used to assess protein quality (polydispersity) and test different storage conditions. A DynaPro NanoStar DLS Detector (Wyatt Technology) was used to perform a measurement on 100 µl protein sample in a disposable cuvette (Wyatt Technology). Each measurement was carried out as a set of 10 sub-measurements each 5 sec long. The measurements were setup and analyzed using the Dynamics 7.5.017 software (Wyatt Technology).

CelluSpots Assay

CelluSpots membrane (Intavis) containing 15 amino acid long peptides of 5 different Z-disk proteins, with adjacent peptides having an overlap of 11 amino acids, was previously designed in the Djinovic lab. The membrane was briefly washed with TBS buffer and incubated with 57 μM Calcineurin for 1 h at RT to allow for potential interaction with membrane spotted peptides. After briefly washing the membrane with TBS buffer, a one hour blocking step with 2% BSA solution followed. The membrane was washed (3x 5 min) with TBST buffer and incubated with mouse 6x His monoclonal primary antibodies (Thermo Fisher Scientific) for 1 h. After washing the membrane (3x 5 min) with TBST buffer, the membrane was incubated with rabbit anti-mouse secondary antibody conjugated with horseradish peroxidase (Abcam) and finally washed (3x 5 min) with TBST buffer. Pierce ECL Western Blotting Substrate (Thermo Fisher Scinetific) was used for detection and chemiluminescence was measured using Fusion-FX7 to visualize the spots.

PullDown Assay

Protein were dialyzed against Buffer PD1 overnight and centrifuged at 4 °C and 186 000 x g for 30 min in the Beckmann ultracentrifuge (rotor TLA-55). Next, protein concentration was measured at 280 nm using the Nano Spectrophotometer. In the first set of experiments, 5 μM Strep-tagged myotilin were mixed with different concentrations of CN (2.5 μM, 5 μM, 7.5 μM and 10 μM) in a total volume of 110 μl. Additionally, samples containing only myotilin were prepared as a control. The sample was incubated for 30 min at RT. As a reference, 10 μl of input sample was taken and prepared for SDS-PAGE. The remaining sample was applied to 25 μl of Strep-tactin resin (IBA) per well, which was pre-equilibrated with Buffer PD1. MICROLABS STAR pipetting robot (HAMILTON) was used to perform the experiment. The sample was then incubated on the resin while constantly shaking at 25 °C for 30 min and washed three times using Buffer PB1. Buffer PB2 was used to elute the proteins. The second set of experiments was performed in the same manner with the exception that His-tagged CN was incubated with different myotilin concentrations (2.5 μM, 5 μM and 10 μM) and applied to a Co^{2+} resin (Thermo Scientific). CN sample prepared without addition of myotilin was used as a control. All eluted and input samples were analyzed on a 15% SDS-PAGE gel.

SEC-MALS

Proteins were dialyzed against the SEC-MALS buffer overnight and centrifugation at 4 °C at 186 000 x g for 30 min in the Beckmann ultracentrifuge. Protein concentration was determined using the Nano Spectrophotometer. To create the complex, 10 μM CN and 30 μM $Myot^{185-489}$ were incubated together in a total volume of 200 μl at 4 °C for 1 h. As references, 10 μM CN alone and 30 μM $Myot^{185-498}$ alone were used. After equilibration of a Superdex 200 10/300 Increase (GE Healthcare) column with SEC-MALS buffer overnight, 100 μl of the sample was injected and experiments were performed at a flow rate of 0.75 ml/min. Agilent 1260 Infinity HPLC system (Agilent Technologies) equipped with miniDAWN® (MALS detector, Wyatt Technology), and

refractive index detector RI-101 (Shodex) was used to perform the experiment. Analysis was performed using the ASTRA 7.1.1 Software.

Isothermal Titration Calorimetry (ITC)

Proteins were dialyzed against the ITC buffer overnight, centrifuged at 4 °C at 186 000 x g for 30 min in the Beckmann ultracentrifuge and their concentration was determined at 280 nm using the Nano Spectrophotometer. Myot$^{185-444}$ (241 μM) was titrated into a cell containing 24 μM calcineurin at RT and 500 rpm using a Malvern Panalytical MicroCal Peaq-ITC instrument. Twenty injections were made in total, at first one 0.4 μl and subsequent nineteen 2 μl injections. Data analysis was performed using the MicroCal Peaq-ITC Analysis Software.

Calcineurin Activity Assay

After ion exchange chromatography of calcineurin, a fraction of each CN containing peak was selected to be tested and CN concentration was measured at 280 nm on a Nano Spectrophotometer. A Micro Bio-Spin 6 Column (BioRad) was used to perform buffer exchange to calcineurin activity buffer. To test CN activity in presence of p-nitrophenyl phosphate (pNPP), reaction triplicates were pipetted into a 96 well plate according to the following pipetting scheme: in a total volume of 150 μl, 1 μM calcineurin was incubated with 2 mM pNPP (Sigma) for at 30 °C 10 min. Absorption was measured at 420 nm in a TECAN plate reader. Additionally, CN activity was also tested in presence of the RII phospho-peptide of the established CN substrate, the cAMP-dependent protein kinase regulatory subunit type II. Reaction triplicates were pipetted into a 96 well plate according to the pipetting scheme; in a total volume of 50 μl, 50 nM CN was incubated with 40 μM RII peptide at 30 °C for 30 min. Reaction was stopped by addition of 100 μl of BIOMOL Green reagent and incubated for additional 20 min to allow enough time for detection of free phosphate. Absorption was measured at 612 nm in a TECAN plate reader and data was analyzed in Microsoft Excel.

Myotilin Dephosphorylation Assay

After ion exchange chromatography of calcineurin, fraction from the first peak was selected and CN concentration was measured at 280 nm on a Nano Spectrophotometer. A Micro Bio-Spin 6 Column (BioRad) was used to perform buffer exchange to calcineurin activity buffer. Additionally, all used peptides (myotilin peptides or the RII peptide) were dissolved in the calcineurin activity buffer. Reaction triplicates were pipetted into a 96 well plate according to the following pipetting scheme: in a total volume of 50 μl, 50 nM CN was tested against different concentrations (78 μM, 39 μM, 19.5 μM, 4.88 μM, 2.44 μM) of either phosphorylated myotilin peptides, RII (used as positive control) or non-phosphorylated myotilin peptide (used as negative control). Wells containing CN alone, each of the peptides at highest concentration alone and buffer alone were used as additional controls. Reactions were incubated for 30 min at 30 °C and stopped by addition of 100 μl of BIOMOL Green reagent and incubated for additional 20 min to allow enough time for detection of released phosphate. Absorption was measured at 612 nm in a TECAN infinite FS60 plate reader (Tecan) and data was analyzed by Microsoft Excel.

AKT Kinase Assay

AKT1 constitutively active kinase domain (100 nM) were incubated with different concentrations (100 µM, 50 µM, 25 µM, 12.5 µM, 6.25 µM, 3.125 µM, 1.56 µM and 0.78 µM) of Myot$^{185-444}$ in the AKT activity buffer at 25 °C in a total volume of 25 µl for 30 min. Additionally, 100 nM AKT alone, 100 µM Myot$^{185-444}$ alone, 100 nM AKT1 in a buffer without $MgCl_2$ and ATP and 100 µM Myot$^{185-444}$ S229D S233D were used as negative controls. Crosstide peptide (50 µM) was used as positive control. To stop the reaction 25 µl ADP-Glo reagent (Promega) were added to the samples and incubated for at 25 °C for 40 min to allow all remaining ATP to be hydrolyzed to AMP and PP. Finally, the sample was incubated with 50 µl of the Kinase Detection Reagent (Promega) at 25 °C for 1 h to allow for conversion of ADP, which was produced during substrate phosphorylation of AKT, to be converted back to ATP and detected in a luciferase-dependent manner. Luminescence was measured without attenuation in a TECAN infinite FS60 plate reader (Tecan) and data was analyzed by Microsoft Excel.

Crystallization of CN with the Myot$^{213-232}$ peptide

For initial screening, gel filtration purified CN was concentrated to 3 mg/ml (46 µM) and centrifuged at 186 000 x g and 4 °C for 30 min in a Beckmann ultracentrifuge (Rotor TLA-55). Myot$^{213-232}$ peptide was dissolved in Buffer C7 and 100 µM were added to CN. The complex was used immediately to set up 400 nl sitting drops at ratio 1:1 of protein to precipitant solution, using a Mosquito pipetting robot (TTP Labtech) with five commercial screens: JCSG, Index, Crystal Screen, PACT and Salt RX in MRC 2-well plates. Crystal optimization was performed with screens designed using the Crystal Track Software (Rigaku) and pipetted using an Alchemist pipetting robot (Rigaku) around five promising conditions, mainly by screening different PEG 3350 concentrations and pH values. For optimization a complex of 2.5 mg/ml (38.5 µM) CN and 100 µM Myot$^{213-232}$ were prepared as previously described and used to set up 3 µl sitting drops at rations 2:1, 1:1 or 1:2 of protein to precipitant solution, using Oryx 8 pipetting robot (Douglas Instruments) with five optimization screens in MRC 2 plates. All plates were stored at 22 °C in the Rock Maker 1000 (Formulatrix) and regularly examined using the Rock Maker 3.9.2.1 Software (Formulatrix).

Structure Determination

X-ray diffraction data were collected on European Synchrotron Radiation Facility (ESRF) beamline ID23-1 using flesh frozen crystals soaked in mother solution containing 25% glycerol. Diffraction data of one crystal were used to solve CN structure by molecular replacement using coordinates of the subunits A and B of the CN heterodimer (PDB code ID 5sve, NFATc1 peptide coordinates were omitted) as a search model with Molrep (CCP4) (Winn et al., 2011). In an iterative approach, model building was performed in COOT (Emsley et al., 2010) followed by refinement in Phenix Refine (PHENIX) using automatically defined TLS groups (Adams et al., 2010). MolProbity (Chen et al., 2010) was used to validate the final structure. All figures of the solved structure were generated in PYMOL (Schröder).

Results

Myotilin purification resulted in high amount of monodisperse sample.

All myotilin constructs were expressed and purified in the same manner and exhibited similar behavior. Thus, using Myotilin 185-444 (Myot$^{185-444}$), which is the wild-type myotilin construct designed for this study, as an example, we describe a typical myotilin purification experiment (Figure 6). A detailed protocol and an overview of all construct can be found in the Materials and Methods section.

Myotilin was expressed in *E. coli* C41 cells and ZYP-5052 auto-induction media at 18 °C overnight. Upon harvesting and lysis, three different purification strategies were used to obtain a pure sample. In the first step, myotilin was isolated from the lysate using nickel-affinity chromatography. Following overnight cleavage with the 3C protease and separation of the cleaved from the un-cleaved portion of the sample in a second nickel-affinity step, cleaved myotilin was purified by cation-exchange chromatography. In the final step, myotilin was eluted from a size exclusion column which resulted in a sharp, symmetric peak. Final yield was high, as approximately 60 mg of myotilin were obtained from 1 l of media. The protein could be concentrated to high values, typically between 8 and 15 mg/ml, showed a single band on SDS-PAGE and displayed properties of a monodisperse sample in all DLS measurements.

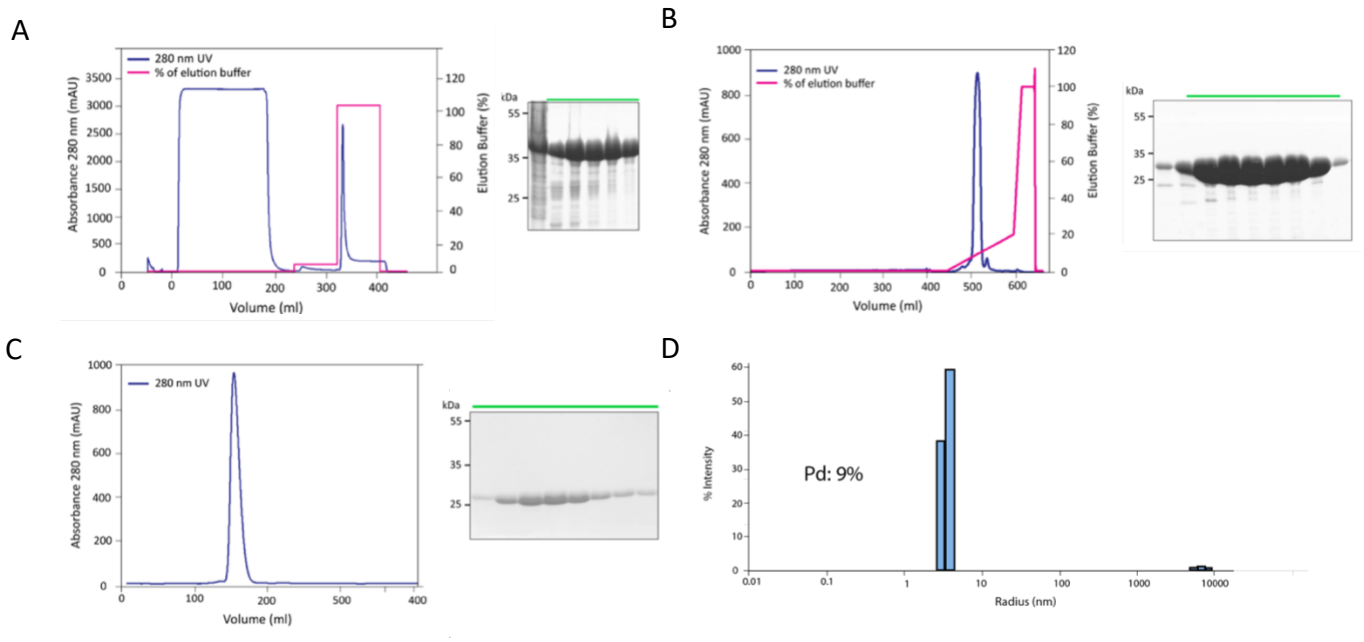

Figure 6. Purification of Myot$^{185-444}$ as an example of all myotilin construct purifications.

Figure shows chromatography profiles and SDS-PAGE assessment of corresponding peak fractions in atypical myotilin purification. The fractions marked with a green line were pulled and used for further purification. (A) Firstly, myotilin was purified using a HiTrap FF crude column, (B) cation-exchange chromatography using a ResourceS column was performed. (C) Finally, myotilin was purified in a gel filtration step using a HiLoad 26/600 Superdex 75 column. (D) DLS profile of the final purification product showed that the sample is monodisperse, as polydispersity was measured to be 9%.

CN purification was adjusted to obtain active and pure CN.

A truncated CNA: 1-391/ CNB: 1-170 (CN) was used to perform all experiments in this study. This construct lacks the disordered C-terminal part of CAN subunit which is responsible for calmodulin binding and autoinhibition. The truncation makes CN independent of activation by calmodulin and increases its stability compared to the full-length protein. The complete protocol and additional information about the construct can be found in the Materials and Methods section.

Two main changes were made to adapt the original preparation procedure of CN, as we encountered issues regarding protein yields and stability. Instead of using LB media, a more nutritious, TB media was used to grow cells expressing CN. Additionally, to achieve better aeration, the usual media to flask volume ratio of 1:4 was changed to 1:8.

CN was purified using three chromatographic steps (Figure 7A, B and C), which were performed consecutively in one day with minimal delay. After purifying the sample using cobalt-affinity chromatography, protein was dialyzed for 1.5 h to achieve a lower salt concentration of the sample. Next, CN was subjected to anion-exchange chromatography and three partially overlapping peaks were obtained. When analyzed by SDS-PAGE, all three peaks contained CN and seemingly the same amount and type of impurities.

To test whether the three ion exchange peaks exhibited different properties in regard to substrate processing, dephosphorylation assays were performed using either pNPP, a small compound routinely used for detection of alkaline phosphatases, or the RII peptide, an established CN specific substrate (Figure 7E and F). Both pNPP and the RII peptide are widely used to test CN activity. The results of both assays were similar: while all three CN peaks exhibited activity, the first peak appeared to be the most active. The second peak displayed lower activity and was only slightly more active than the third one. Although the most active, the first peak could not be used alone, as previous experiments showed that the protein became unstable after gel filtration. Thus, to obtain an active and stabile sample, the first two ion-exchange peaks were pooled together and applied onto a size exclusion column. As a result, two CN peaks were eluted; the first smaller peak corresponded to aggregated protein, followed by a larger peak containing soluble, pure CN. Around 8 mg of CN were obtained per 1 l of media from a typical purification experiment. The protein was concentrated to 2 to 4 mg/ml as the sample would aggregate at higher values. The optimal concentration for a well behaving sample was around 2.5 mg/ml. At this concentration, prior to freezing, CN appeared monodisperse when analyzed using DLS (Figure 7D).

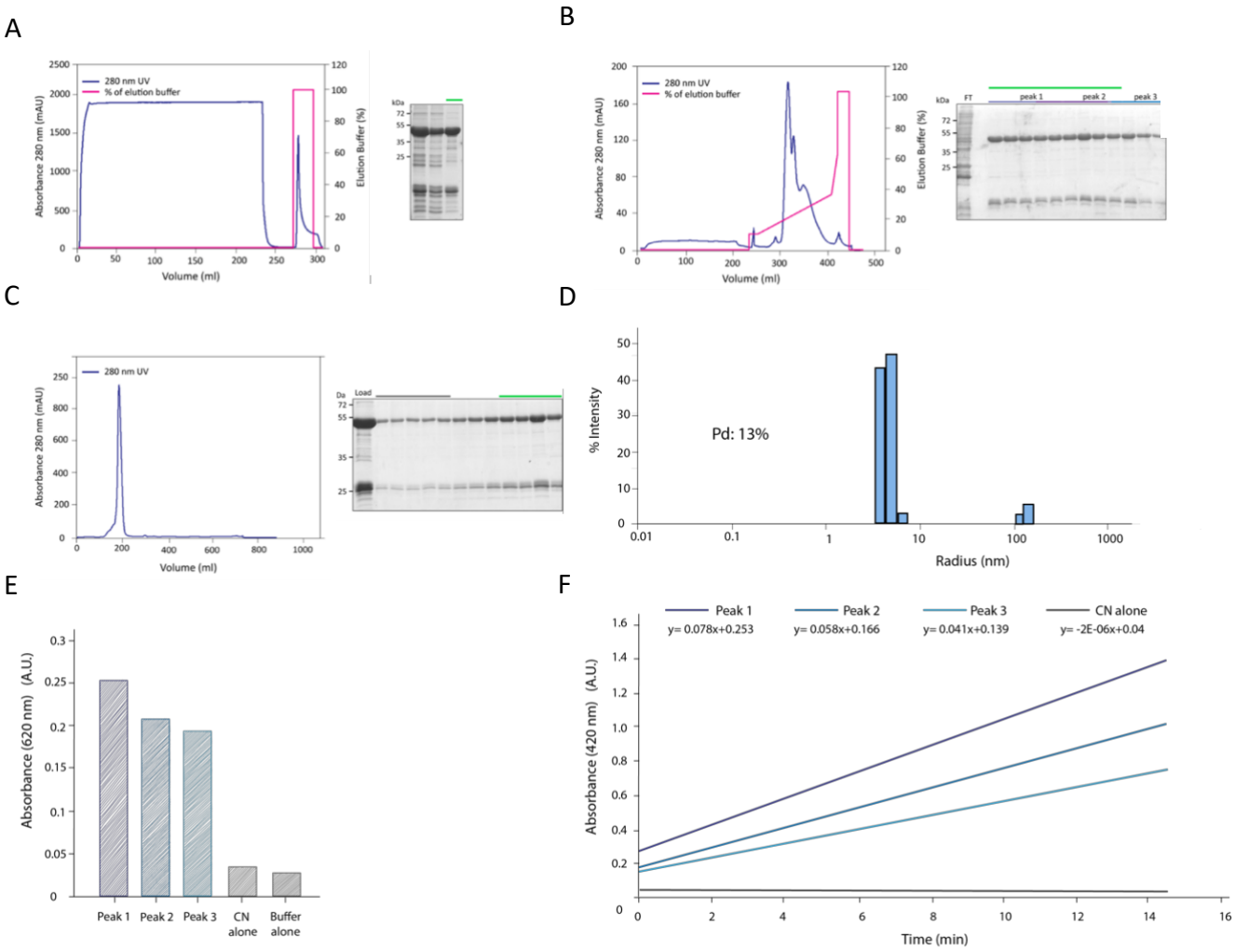

Figure 7. Purification of truncated CN A: 1-391/B: 1-170 (N-His).

Figure shows chromatography profiles and SDS-PAGE assessment of corresponding peak fractions in atypical myotilin purification. The fractions marked with a green line were pulled and used for further purification. (A) CN was purified using a HiTrap Talon crude column. (B) Ion-exchange purification followed using a ResourceQ column. The gray lines represent different ion-exchange peaks which all contained CN. (C) Finally, a size exclusion chromatography was performed using a HiLoad 16/600 200 column. (D) DLS profile of the final purification product showed that the sample is monodisperse, as polydispersity was measured to be 13%. (E) The first set of dephosphorylation assays was performed using 1 μM CN from a fraction of one of the ion exchange peaks and 2 mM pNPP. Absorption was measured at 420 nm over 15 min to monitor dephosphorylation. CN in the first peak (blue) displayed highest activity, followed by the second peak (orange) and third peak (gray). CN without any pNPP was used as a negative control (yellow). (F) A similar outcome was obtained in the second set of dephosphorylation assays in which 50 nM CN and 40 μM RII peptide were used. After incubation the reaction for 30 min, the reaction was incubated with BIOMOL Green to detect dephosphorylation at 620 nm.

A DLS test revealed that CN is prone to aggregation after freezing.

Freezing and thawing seemed to have a detrimental effect on the sample. To investigate this thoroughly, CN was frozen and thawed, afterwhich a series of steps including sample concentration, ultracentrifugation, size exclusion chromatography and another protein concentration followed. After each step, DLS we measured to assess sample monodispersity (Figure 8). Polydispersity of the sample increased after thawing and concentrating, indicating aggregation of the sample caused by freezing (Figure 8B), indicating aggregation of the sample caused by freezing. Although CN was more monodisperse after ultracentrifugation (Figure 8C),

there was indeed, a fraction of sample that was lost due to aggregation, which was observed when the supernatant and the pellet was analyzed by SDS-PAGE after ultracentrifugation (Figure 8A). Once eluted from the size exclusion column, both individual and pooled protein fractions appeared more monodisperse (Figure 8D and E). Finally, leaving the sample overnight at 4 °C lead to sample destabilization, as three instead of two populations were observed in DLS (Figure 8F). Although the protein could be reused, there was a noticeable decrease in sample stability upon freezing and thawing. Hence, to work with the sample of highest quality, CN was freshly prepared before each experiment and used immediately after purification without freezing. A summary of the test in given in Figure 8.

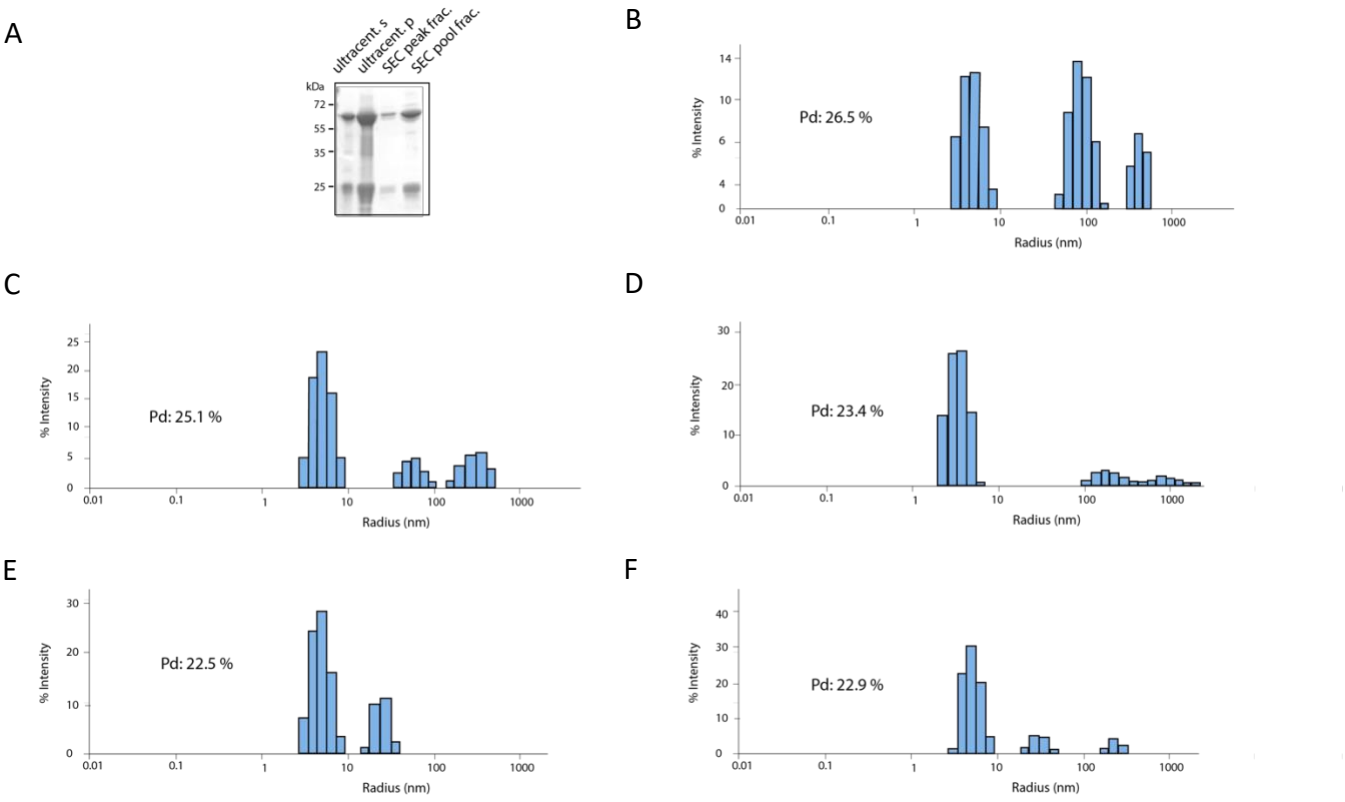

Figure 8. Storage condition test performed using DLS.
Shown are DLS profiles of different steps of sample regeneration after freezing and thawing the sample. (A) SDS-PAGE of CN samples taken at selected steps of the process: lane 1- the supernatant after the first ultracentrifugation, lane 2- pellet after the first ultracentrifugation (significant sample loss), lane 3- highest size exclusion fraction, lane 4- pooled size exclusion fractions. (B) DLS profile of the sample after thawing shows polydispersity of 26.5%, (C) After the sample has been concentrated and ultracentrifuged, the polydispersity was measured to be 25.1%, (D) The sample was next loaded on a size exclusion column and polydispersity of the highest peak fraction was determined to be 23.4%, (E) After pooling the fractions, concentrating and spinning the sample, the polydispersity was 22.5%, (F) Finally, after leaving this sample overnight at 4 °C the measured polydispersity was at 22.9%.

Calcineurin and myotilin interact. The disordered N-terminal half of myotilin plays a role in this interaction.

To establish whether myotilin interacts with CN, we performed pulldown experiments. Firstly, we analyzed whether CN would bind to Myot$^{185-498}$ which was immobilized to Strep-tactin beads (Figure 9). For this experiment 5 μM Myot$^{185-498}$ was incubated with increasing concentrations of CN (2.5 μM, 5 μM, 7.5 μM, 10μM). A binding of CN to Strep-tagged Myot$^{185-498}$ was detected by

SDS-PAGE and the band corresponding to CN became more prominent when higher CN concentrations were used, indicating that more complex had been formed on the beads. This was not the case in the control, where very faint CN bands were detected, showing that CN was barely retained on Strep-tactin beads in absence of Strep-tagged Myot$^{185-498}$.

.

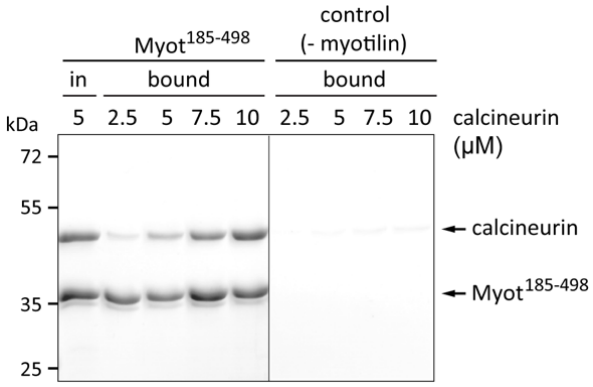

Figure 9. Pulldown of CN with Myot$^{185-498}$ bound to Strep-tactin beads.

Strep-tagged Myot$^{185-498}$ (5 μM) was incubated with increasing concentrations of CN (2.5 μM, 5 μM, 7.5 μM and 10 μM). The sample was applied to Strep-tactin beads, incubated, washed and finally eluted to investigate the binding of the two proteins. The figure shows input and elution fractions analyzed by SDS-PAGE. A fraction from the input sample where Myot$^{185-498}$ and CN were mixed in a 1:1 molar ration was loaded in the first lane. The following lanes (bound) show fractions of the sample which was eluted from the beads. The first four lanes correspond to samples where myotilin was mixed with CN. These show concentration-dependent enrichment of CN in presence of Myot$^{185-498}$. No such enrichment was observed in the next four lanes (control lanes), where CN was incubated and tested in absence of Myot$^{185-498}$.

Next, to verify our finding, we performed complementary experiments, where we tested whether Myot$^{185-489}$ would interact with CN bound to Co^{2+}-Sepharose beads (Figure 10A). The assay was performed as before, as the concentration of the immobilized protein, the His-tagged CN in this case, was kept at 5 μM and the concentration of the non-tagged protein, myotilin, was varied (2.5 μM, 5 μM and 10 μM). As in our previous experiment, the two proteins interacted, and the binding became more prominent when higher amounts of Myot$^{185-489}$ were used. Finally, in an attempt to narrow down the region of myotilin responsible for CN binding, we investigated whether Myot$^{250-489}$, a myotilin construct which lacks the N-terminal disordered half, would also interact with CN (Figure 10B). Although some Myot$^{250-489}$ remained bound to Co^{2+}-Sepharose beads primed with CN, we did not detect a clear enrichment, comparable to the one observed when Myot$^{185-489}$ was used. Notably, both Myot$^{185-489}$ and Myot$^{250-489}$ exhibited some unspecific binding to bear Co^{2+}-Sepharose beads. Altogether, our pulldown experiments show that myotilin and CN interact and suggest that the N-terminal region before the first Ig domain of myotilin is responsible for this binding.

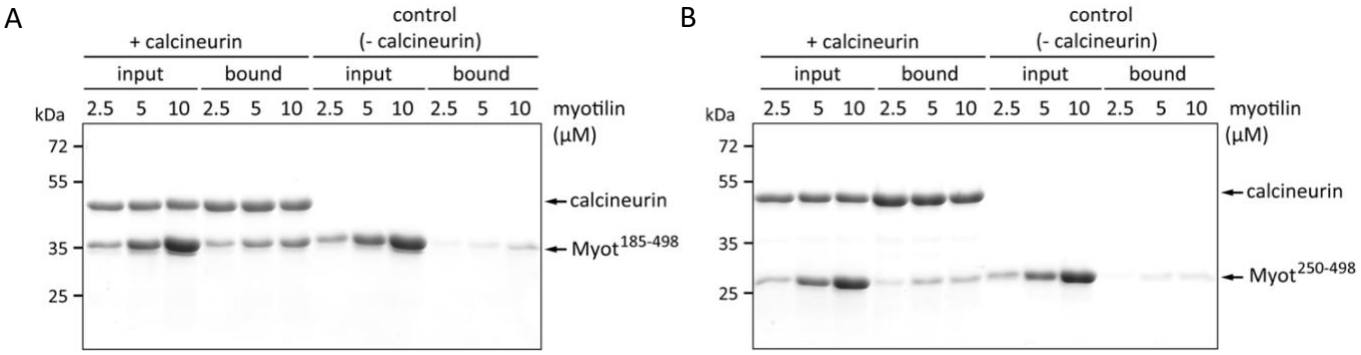

Figure 10. Pulldown of Myot$^{185-498}$ and Myot$^{185-250}$ with CN bound to Co-Sepharose beads.

Myotilin and CN were mixed, applied to Co^{2+}-Sepharose beads, incubated, washed and finally eluted to investigate the binding between the two proteins. The figure shows input and elution fractions analyzed by SDS-PAGE. (A) Pulldown was performed by incubating His-tagged CN (5 μM) with increasing concentrations of Myot$^{185-498}$ (2.5 μM, 5μM, 10μM). Fractions from the input sample were loaded in the first three lanes. The rest of the input sample was applied to the beads, incubated and eluted. Fractions of eluted samples were loaded in the following three lanes and show interaction between CN and Myot$^{185-498}$. Finally, only faint bands of Myot$^{185-498}$ were detected in the last three control lanes, where CN was not present in the sample. (B) The same experiment was repeated with His-tagged CN (5 μM), but this time Myot$^{250-498}$ (2.5 μM, 5μM, 10μM) was used. Myot$^{250-498}$ interacted with CN less strongly and no concentration-dependent enrichment was observed in lanes containing eluted fractions. Additionally, some unspecific binding of Myot$^{250-498}$ with the beads was detected, as seen in control lanes.

Myotilin binds CN via ^{220}LQVP^{223} which resembles the LxVP CN binding motif.

In our pulldown experiments, we identified the disordered N-terminal part of Myot$^{185-489}$, as a region important for binding to CN. To investigate if there are other regions contributing to this interaction and map the exact site on myotilin to which CN bind, we conducted a CelluSpots peptide array assay. In the peptide assay, a membrane which contained protein sequences of 5 different Z-disk proteins including myotilin, FATZ and partial sequences of ZASP, Filamin C and Xin, was incubated with His-tagged CN. Proteins were spotted on the membrane in form of 15 residue-long peptide, and every peptide overlapped by 11 residues with its adjacent neighbor. Upon detection of CN with anti-His-tag antibodies, five prominent spots were visualized (Figure 11A). Two of the five detected spots corresponded to His-control peptides (Figure 11B). Additionally, three adjacent peptides were detected in the membrane region where myotilin peptides were spotted (Figure 11B). These peptides corresponded to a region spanning residues 209 to 231 found in the N-terminal part of Myot$^{185-489}$, which confirmed the importance of this region for CN binding (Figure 11C).

Notably, ^{217}HARLQVP^{223} was the minimal sequence shared by all three detected peptides (Figure 11B). The LQVP resembles closely the LxVP motif found in the binding site of many described CN interaction partners (Figure 11D). The LxVP motif has previously been established as the second short linear motif, alongside PxIxIT, which CN uses to recognize and bind its various substrates and regulators (Park et al., 2000). Therefore, we speculate that the ^{220}LQVP^{223} sequence of myotilin is the LxVP motif responsible for CN binding.

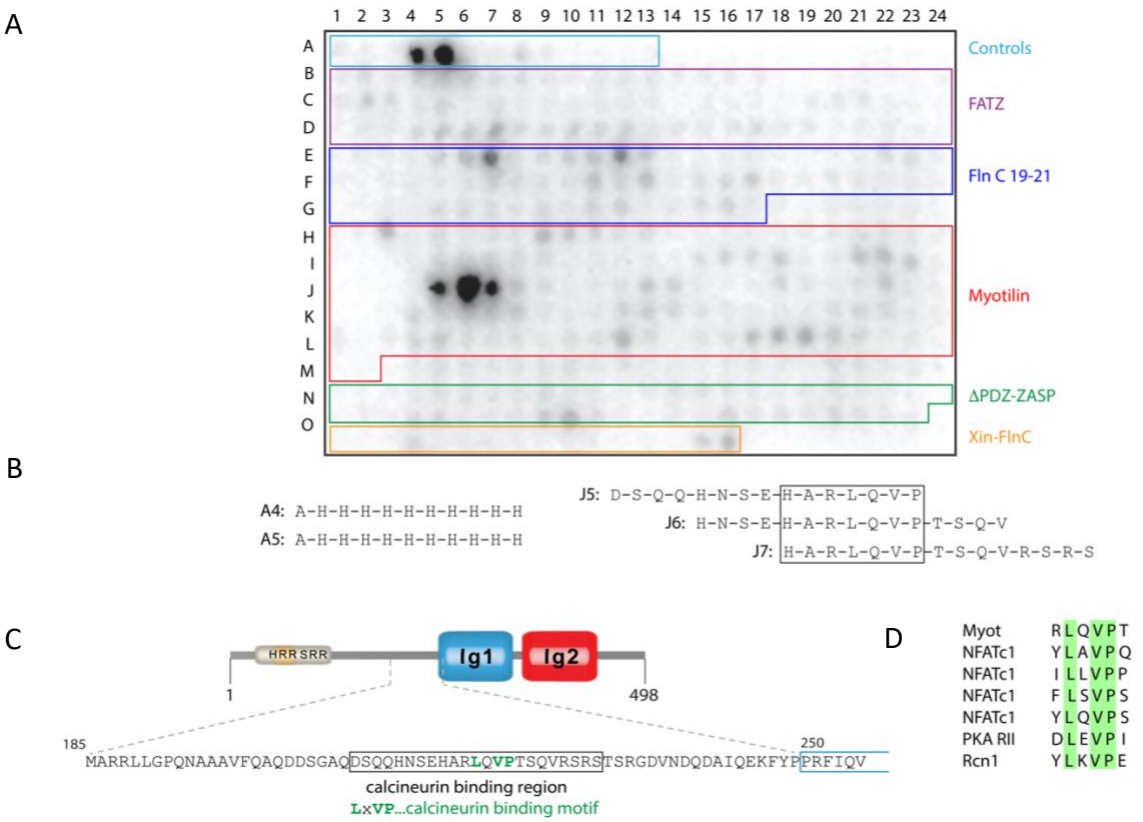

Figure 11. CelluSpot peptide array assay

(A) CelluSpot membrane contains controls (light blue) and sequences of five Z-disc protein, FATZ (purple), filamin C domain 19-21 (dark blue), myotilin (red), ZASP lacking the PDZ domain (green) and FlnC binding region of Xin (orange), in form of spotted 15 amino-acid long peptides. Five strong spots were recognized: two belonging to the control His-tag sequence, three belonging to myotilin. (B) Sequences of the five detected peptides: two deka-His tag peptides and three corresponding to myotilin. (C) Myotilin has two Ig domains and a disordered N- and C-terminal region. Detected peptides correspond to the myotilin region (in box) found in the disordered N-terminal part close to the first Ig domain. This sequence contains the LxVP motif (green) which is known to be recognized by CN. (D) Alignment of LxVP motifs of known CN substrates and myotilin.

The interaction between calcineurin and myotilin is in the low micromolar range, indicating a substrate-enzyme interaction.

Once we determined the exact region of myotilin that interacts with CN, we wanted to characterize the myotilin-CN complex. In our pulldown assays, we observed complex formation at fairly low concentrations of the two binding partners, implying that this complex is stable. However, in a solid based assay, the binding could be enhanced due to high local concentrations and unspecific interaction with the beads. Thus, to analyze a myotilin-CN complex formed in solution, we performed SEC-MALS. SEC-MALS was used to analyze complex formation and determine binding stoichiometry. Myot$^{185-489}$ and CN were first loaded separately, and molecular weights obtained from these control runs, namely 68.3 kDa and 35.9 kDa, was in good agreement with the expected molecular weights of one CAN-CNB heterodimer and one Myot$^{185-489}$ molecule, respectively (Figure 12). Additionally, CN displayed a small peak corresponding to a molecule of 151.2 kDa. Although this matches the size of a theoretical CN dimer, this oligomerization is unspecific as no such CN dimer was ever characterized. Next, we analyzed the complex prepared by incubating CN with Myot$^{185-489}$. Upon elution, we observed two merging peaks, with molecular weight values very similar to the ones measured in control experiments. Moreover, an overlay of

elution profiles obtained from all three runs showed there was no clear shift of the two peaks detected when the complex was analyzed, compared to peaks obtained from individual proteins. Finally, we concluded that the myotilin-CN was not strong enough to survive gel filtration and as a result, we could not determine its stoichiometry.

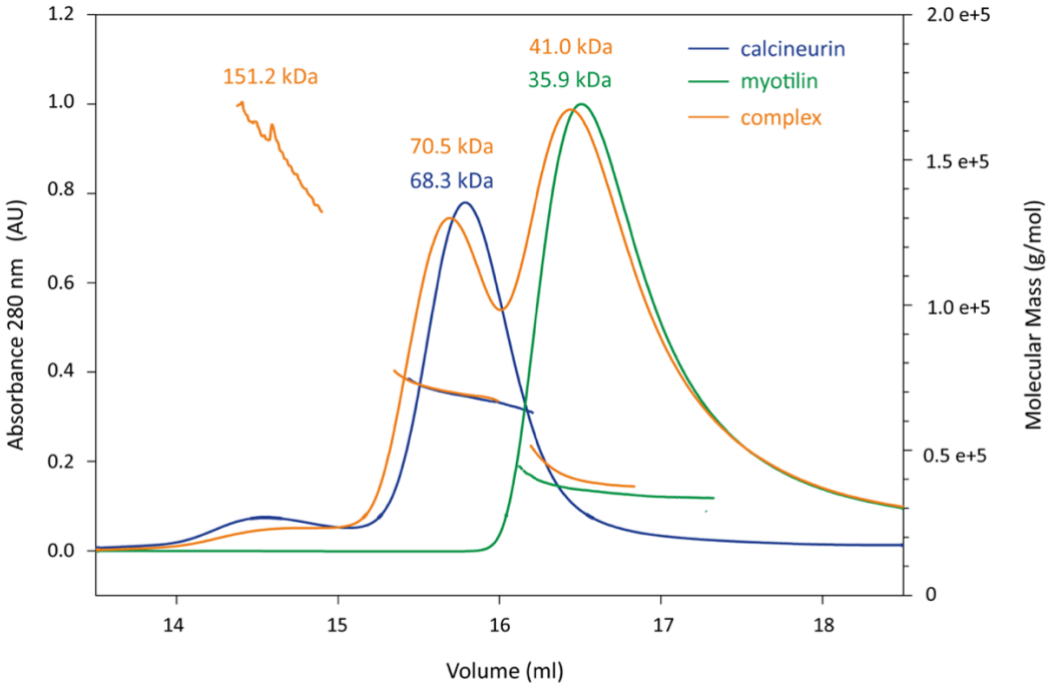

Figure 12. SEC-MALS of CN, Myot$^{185-489}$, and the CN-Myot$^{185-489}$ complex

SEC-MALS was performed with 30 μM myotilin (green), 10 μM CN (blue) and a complex of myotilin and CN at final concentration 30 μM and 10 μM respectively (orange). While molecular weight values correspond well with theoretically determined ones, no stabile complex between CN and myotilin was detected on SEC-MALS indication that the interaction was not strong enough.

To quantitatively characterize the interaction between CN and myotilin and determine the dissociation constant (K_D), we performed ITC. For this purpose, we designed a new myotilin construct, Myot$^{185-444}$, which lacked the C-terminal disordered region. This made the protein more stable and soluble. Obtaining a smaller, well behaving myotilin construct also meant that we could concentrate it to high values and use it as a titrant. This was crucial for performing our ITC experiments, as this was not the case for CN. ITC analysis of the myotilin-CN complex resulted in a K_D of 6.87 +/- 2.3 μM (Figure 13A and B). The ITC data also showed that the interaction between myotilin and CN is driven solely by favorable enthalpic contribution (Figure 13C). Thus, our ITC measurements confirm that the complex formed between myotilin and CN is not a highly stable interaction with a dissociation constant in a low micromolar range. Furthermore, this indicated that the interaction between myotilin and CN resembled more a temporary substrate-enzyme, than a stable inhibitor-enzyme interaction.

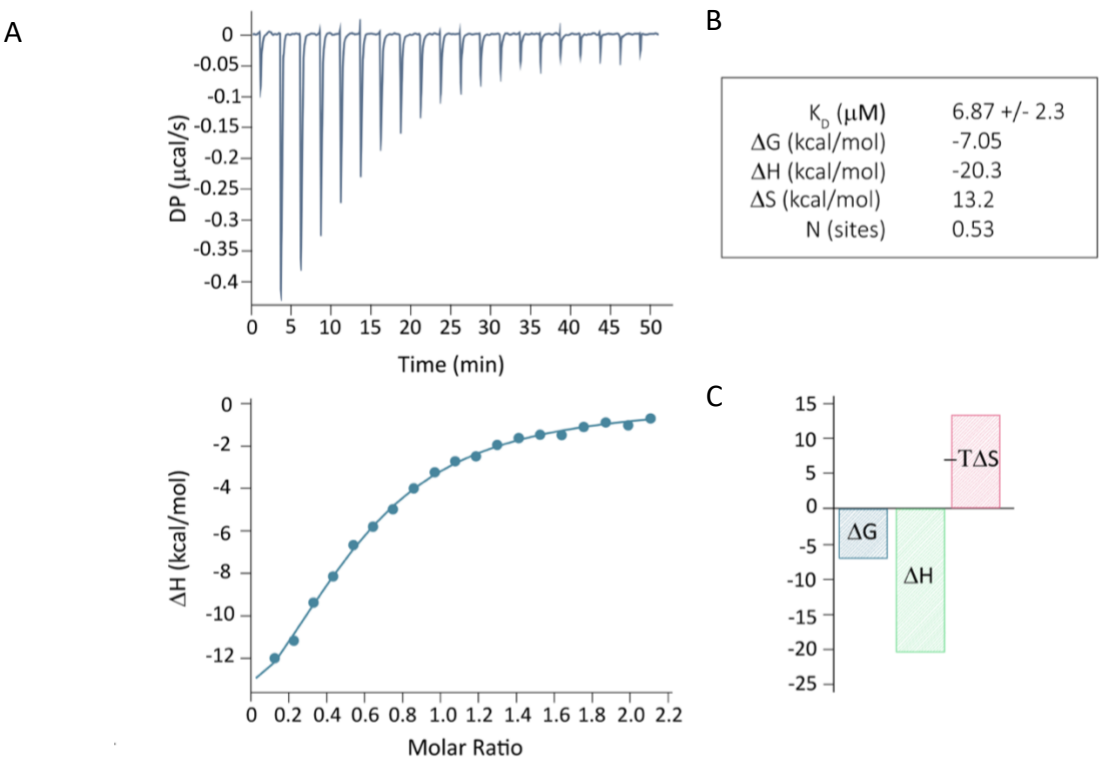

Figure 13. ITC of CN and Myot$^{185-444}$

(A) Raw and interpolated ITC data obtained from the ITC PEAQ Software. ITC was performed by titrating approximately 10-fold higher concentrations of myotilin (around 270 µM) into a cell containing CN (around 23 µM). Three independent measurements were performed to obtain a K_D of 6.87 +/- 2.3 µM. (B) Important ITC parameters are summarized in a table. (C) A bar plot showing contribution of changes in enthalpy and entropy to the final free energy of binding.

Myotilin interacts with CN in a manner characteristic for all LxVP bearing CN binding partners.

To further characterize the myotilin-CN complex and to understand the molecular mechanisms that underlay its formation, we co-crystalized CN with a myotilin peptide. Since our previous experiments revealed that the binding of myotilin to CN was not strong enough to obtain a stable complex, using a myotilin peptide instead of a protein construct was a more suitable choice. Additionally, myotilin contains long disordered stretches which could impair the crystallization process. Thus, to obtain a stable, stoichiometric complex with CN, we used the Myot$^{213-232}$ peptide, which was based on the strongest peptide detected in the CelluSpot peptide array assay (Figure 11B).

As a result of the initial screening, promising hits with needle shaped crystals were obtained after one day in several commercially available conditions. Optimization around these conditions and adjustment of CN concentration, yielded in multiple, elongated three-dimensional crystals (Figure 14A). The structure of CN in complex with Myot$^{213-232}$ peptide was determined from a single crystal (20% PEG 3350, 0.2M ammonium citrate, 0.1M Tris pH 8.5) at 2.77 Å. Crystals formed in space group $P2_12_12_1$, with unit cell dimensions a= 58.01 Å, b= 110.8 Å, c= 115.7 Å, αβγ= 90 ° and contained one CAN-CNB heterodimer bound to one Myot$^{213-232}$ in the asymmetric unit (Table 4).

Collection		Refinement	
Synchrotron beamline	ESRF ID23-1	Resolution range (Å)	46.967 – 2.77

Space group	$P2_12_12_1$	R_{work} (%)	0.1935 (0.3393)
a, b, c (Å) α =β = γ (°)	58.0, 110.8, 115.7, 90	R_{free} (%)	0.2266 (0.3698)
Wavelength (Å)	0.9724	Reflections used in refinement	19424 (1867)
Resolution range (Å)	38.42-2.77 (2.86 -2.77)	Reflections used for R_{free}	944 (85)
Total Reflection	81047	Number of non-hydrogen atoms	4385
Unique Reflection	19428 (1867)	Rmsd Bond length (Å)	0.004
Completeness (%)	99.5 (99.8)	Rmsd Bond angles (°)	0.90
Multiplicity	4.2 (4.3)	Ramachandran favored (%)	96.03
R_{merge} (%)	6.4 (110.9)	Ramachandran allowed (%)	3.97
$R_{p.i.m.}$ (%)	0.1 (0.9)	Ramachandran outliers (%)	0.00
$CC_{1/2}$ (%)	100 (40)	Rotamer outliers (%)	0.00
$I/\sigma(I)$	12.7 (1.0)	Clashscore	2.34
Wilson B-factor (Å^2)	82.6	Average B-factor (Å^2)	96.68

Table 4. Crystallographic table 1

Crystallographic table 1 shows collection and refinement parameters used to obtain the structure of the CN-Myot$^{213-232}$ peptide complex.

The structure of the CN molecule in our model is similar to previously published structures of both CN alone and in complex with its various inhibitors and substrates (rmsd values between 0.509 and 0.858 for comparison of our model with PDB entries 4f0z, 1aui, 1m63 and 1tco), (Figure 14B). Although there was density present at the site where the active metal ions, Fe and Zn are coordinated in the active center, including the atoms led to an increase in the R_{free}. It is not uncommon for deposited CN structures to lack the active center ions. In all analyzed structures including the structure solved in this work, the active center residues which coordinate the metals are positioned the same in all structures regardless if the metals were modelled or not. Four Ca^{2+} ions are bound by the four EF-hand motifs of the CNB subunit. Myot$^{213-232}$ interacts with CN in a manner typical to other characterized LxVP motif bearing peptides: it adopts an extended conformation to bind to a previously described, shallow hydrophobic pocket on the surface of the CNA-CNB interface (Figure 14C) (Grigoriu et al., 2013; Rodriguez et al., 2009).

A

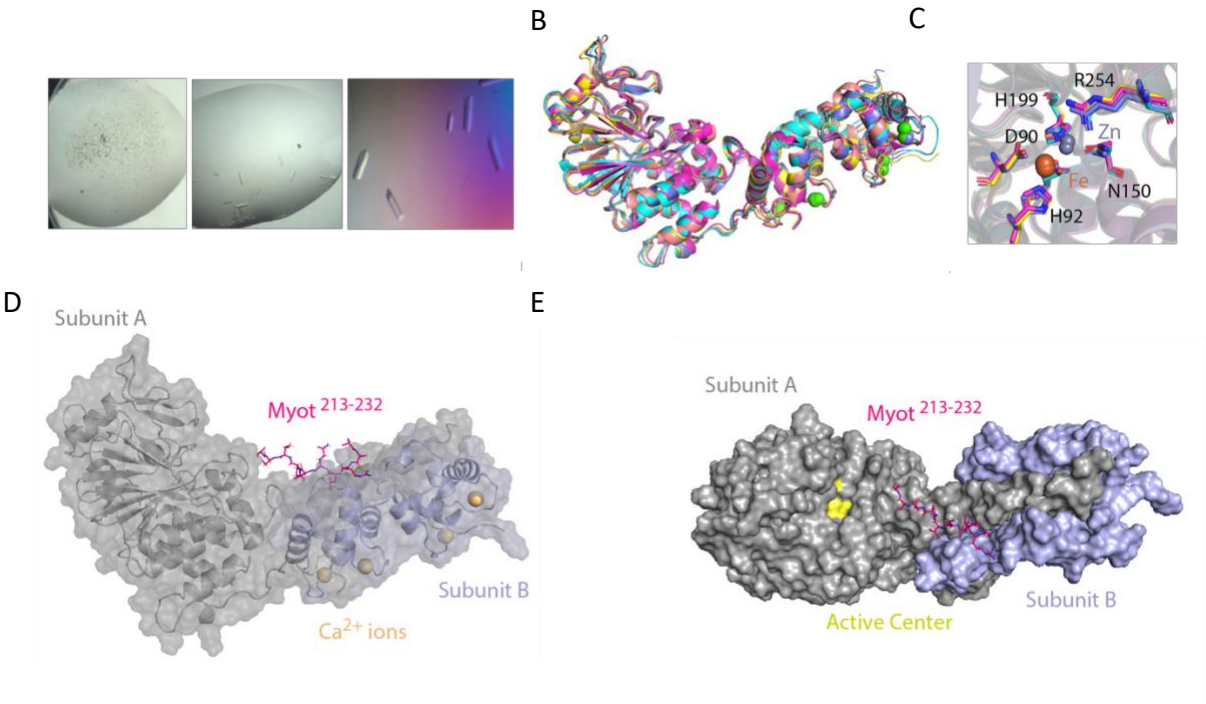

Figure 14. Crystallization of the CN in complex with the Myot$^{213-223}$ peptide.

(A) For initial screening 3 mg/ml CN were mixed with 100 μM Myot$^{213-232}$. Best results were obtained from the JCSG commercial screen condition containing 0.2 M ammonium citrate and 20 % PEG 3350. Elongated, regular crystals were obtained in an optimization screen using 2.5 mg/ml CN and 100 μM Myot$^{213-232}$ in a condition containing 20% PEG 3350, 0.2M ammonium citrate and 0.1M Tris pH 8.5 (B) Superposition of the solved CN structure (cartoon, purple) with four previously deposited structures of CN, 1tco (cyan), 1m63 (salmon), 1aui (yellow) and 4f0z (magenta). (C) Representation of the five main residues of the active center, namely Asp90, His92, His199, Asn150 and Arg254 (sticks) of all aligned structures. Three of the structures (1tco, 1m63 and 1aui) were solved with metal ions in the active center Fe (orange) and Zn (yellow). Although our CN structure, along with the 4f0z, does not have the metals modeled in the active center, the residue positioning is the same in all structures. (D) Structure of the CN heterodimer (cartoon). Catalytic subunit A (gray) and regulatory subunit B (purple) form the CN heterodimer. The interface between the two subunits provides a binding site for Myot$^{213-232}$ (stick, magenta). Four Ca^{2+} ions (sphere, orange) are bound to CNB. (E) Structure of the CN-Myot$^{213-232}$ peptide complex (surface representation). The Myot$^{213-232}$ peptide (magenta) adapts an extensive conformation upon binding to the interface built by catalytic subunit A (gray) and regulatory subunit B (purple). The active center of CN (yellow) is located in the catalytic subunit A.

Not all residues are present in the final structure; electron density was not present for CNA residues 1-44/404-428 as well as CNB residues 1-6 and they were not included in the final model. Additionally, electron density is also absent for residues 213-217 and 226-232 of the Myot$^{213-232}$ peptide. We attribute the lack of electron density of these peptide regions to them not being involved in the interaction and thus, retaining flexibility upon complex formation. Only the mainchain of the first and the last visible peptide residues, His217 and Q226 respectively, was included in our model, since no clear density was observed for their sidechains (Figure 15A).

Finally, the ten myotilin residues, which are visible in our final model, (Figure 15A) are sufficient to describe the interaction between myotilin and CN. Myotilin uses its LxVP motif to bind to a mainly hydrophobic groove at the CNA-CNB interface. Leu220 and Val222, form interactions with multiple residues in the hydrophobic pocket of CN (Figure 15B) and are crucial for myotilin binding to CN.

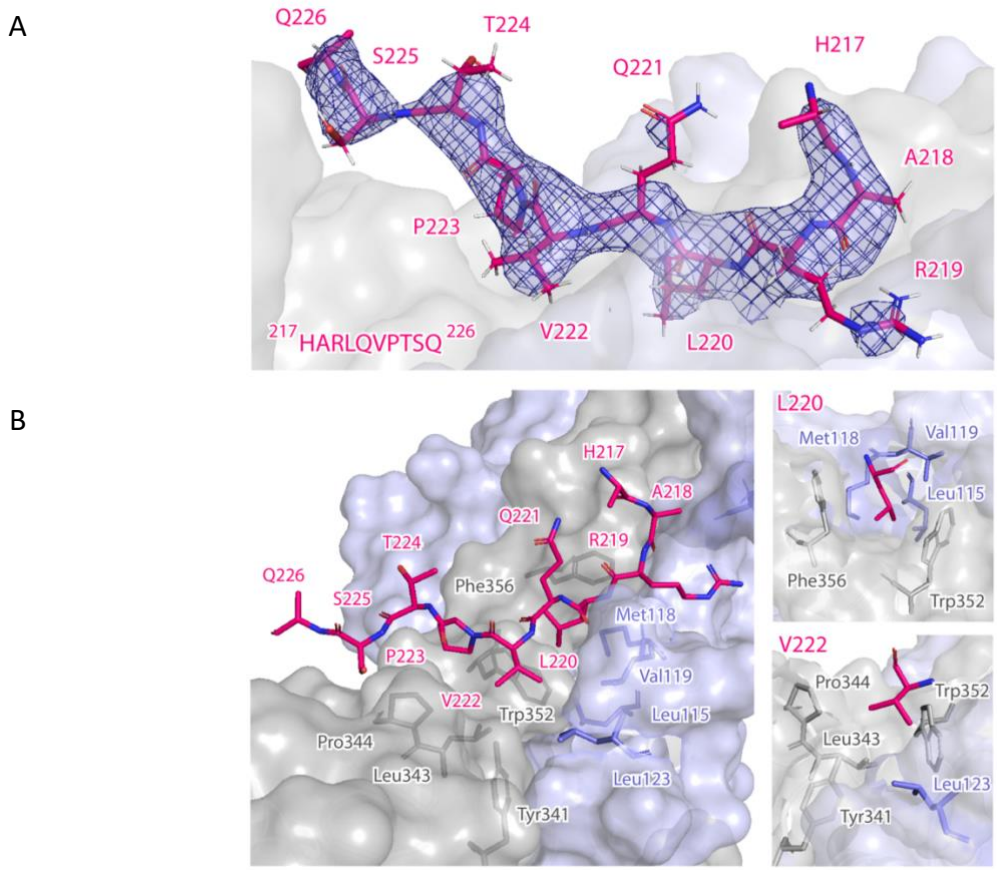

Figure 15. Density and the interactions of the Myot$^{213-223}$ peptide.

(A) Ten residues of the peptide were modeled in the final structure. The density (2Fo-Fc, σ=1.0) is well defined for the main chain and most of the sidechains. No sidechain density is visible for the first and the last modeled myotilin residue, presumably due to flexibility. Additionally, Q221 sidechain displays poorly defined density. (B) Closer view of the modeled myotilin peptide interacting with the hydrophobic groove found on the interface of CNA-CNB heterodimer. Residues L220 and V222 of the LxVP motif are mainly responsible for establishing interactions with hydrophobic residues of CN.

Gln221, the "x" residue of the LxVP motif, does not contribute to binding and its sidechain seems to be flexible, displaying very week electron density compared to the well-defined sidechain densities of the three canonical residues of the LxVP recognition motif. This structure confirms our finding that the LxVP motif is responsible for myotilin recognition by CN and suggests that myotilin interacts with CN in a manner characteristic for other LxVP bearing CN binders.

Myotilin is a substrate of Calcineurin.

The structure of CN in complex with the myotilin peptide confirmed that myotilin uses its LxVP motif to interact with CN and our SEC-MALS and ITC data showed the affinity with which they interaction in not very high. Together, they suggest that myotilin is a substrate of CN, rather than its inhibitor. To support this notion, three different myotilin residues, Ser229, Ser231 and Ser233, found in proximity of its CN binding motif, have recently been shown to be phosphorylated. Two of these serines, Ser231 and Ser233, satisfy the theoretically defined prerequisites for being a CN substrate (Sheftic et al., 2016). Firstly, they are both located more than 6 residues away from the LxVP motif and can reach the active site under assumption that myotilin remains extended. Secondly, they both contain an N-terminally located Arg residue (at position -3 of the

phosphorylated serine), which is proposed to facilitate phosphor-serine positioning in the CN active site (Grigoriu et al., 2013). Ser229 does not contain an Arg residue at position -3, but at position -1 and is located exactly 6 residues away from the LxVP motif (Figure 10C). Additionally, 16.6 Å separate the last peptide residue in our structure from the active site of CN. Since it was not clear that Ser229 could reach the active site, we explored this by modeling a peptide extension in our structure (Figure 16). Indeed, based on this model, phosphorylated Ser229 is able to reach the active site if the region bearing the LxVP motif and this serine remain disordered.

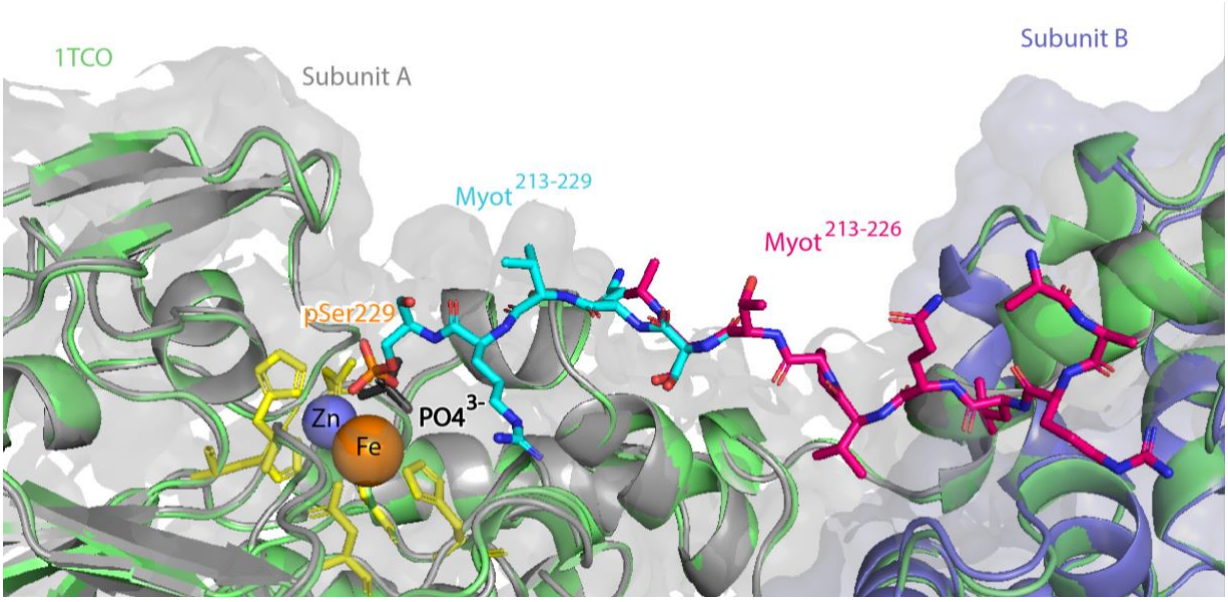

Figure 16. Modeling of the prolonged Myot$^{213-232}$ with the pS229 in the active center.

Myot$^{213-232}$ peptide was built in the visible density until residue 226 (sticks, magenta). To test whether pSer229 can reach the active site, the peptide was model further past the visible density using COOT (sticks, cyan). The last residue modeled is a Ser229 bearing a phosphorylation (sticks, orange and red). The solved CN structure (cartoon, gray and purple) was aligned to the 1tco CN structure (cartoon, mint green) which was salved with the Fe (orange) and Zn (purple) metals bound to a free phosphate (sticks, black) in the active center (sticks, yellow). The phosphate of pSer229 can presumably reach the active center and can be positioned similarly as the free phosphate bound by the active center in the 1tco reference structure.

Therefore, we used three myotilin peptides, each bearing phosphorylation at one of the three potential target serine residues, to determine whether myotilin is a substrate of CN (Figure 17A). Dephosphorylation assays were carried out by incubating different concentrations of each phospho-peptide with CN. Release of free phosphate was detected in the case of all myotilin phospho-peptides, indicating dephosphorylation by CN (Figure 17B). Only basal activity was detected in control wells where CN was incubated with different concentrations of the non-phosphorylated myotilin peptide. RII peptide, an established CN substrate, was used as a positive control to confirm CN activity.

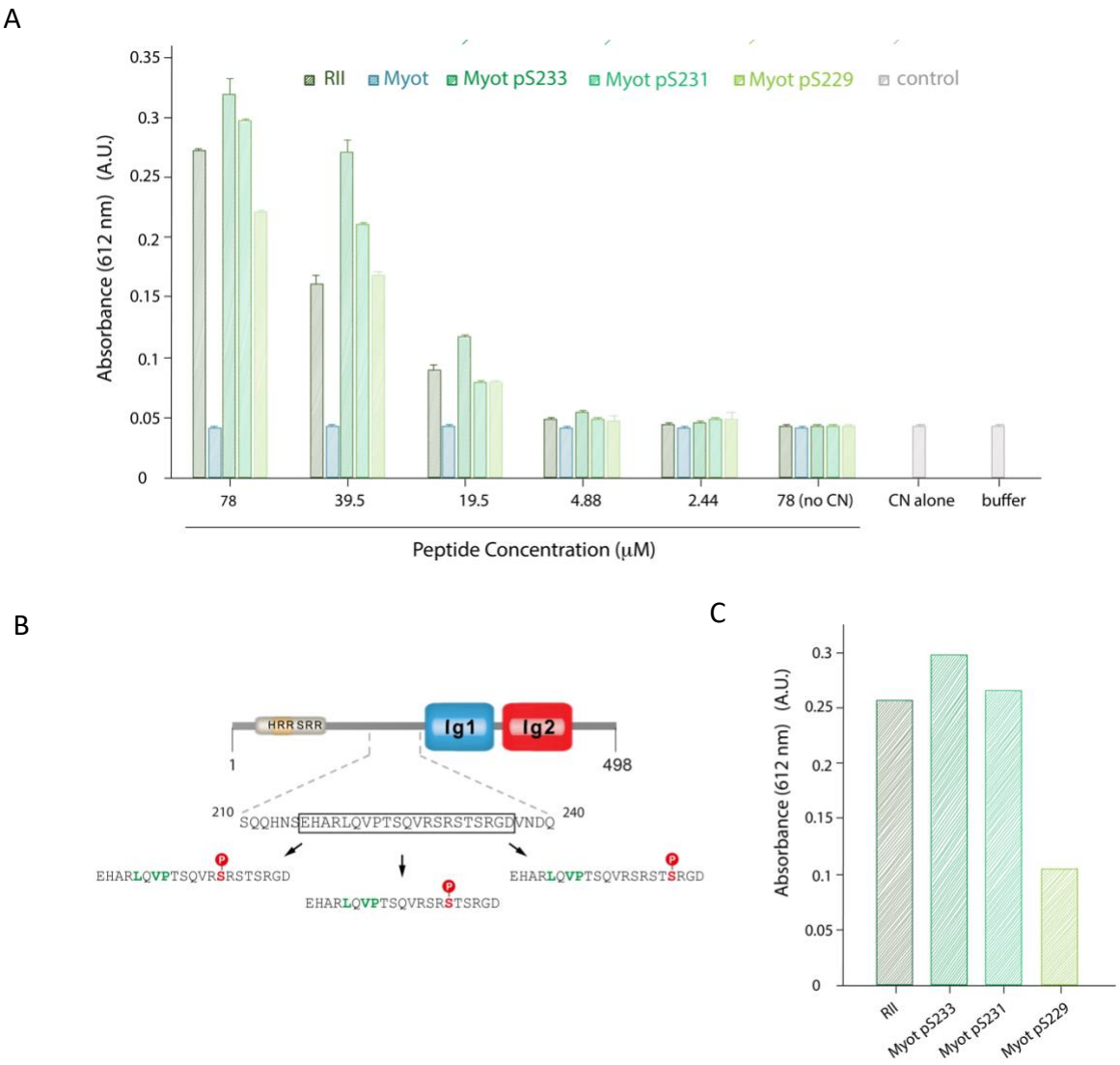

Figure 17. CN mediated dephosphorylation of the myotilin peptides.

(A) Schematic representation of the three peptides bearing the LQVP motif (green) and phosphorylated serine residues (red). (B) Dephosphorylation of phosphorylated myotilin peptides by CN. Plot of substrate concentration-dependent change in absorbance values measured at 612 nm, indicative of the amount of free phosphate released during the reaction. The RII peptide was used as a positive control, non-phosphorylated myotilin peptide was used as a negative control. (C) Comparison of phosphorylation of the myotilin peptides after 15 min. Preliminary results of a dephosphorylation assay carried out using 50 nM CN and 40 μM of different myotilin peptides stopped after 15 min. While the myotilin peptides containing either a phosphorylated Ser231 or Ser233 seem to be dephosphorylated in a similar rate as the RII peptide, which was used as a positive control, the peptide containing a phosphorylated Ser229 is presumably phosphorylated slower and the absorption signal measured in the case of this peptide is almost three-fold lower than for the other peptides used in this assay.

Interestingly, although CN dephosphorylates all three myotilin phospho-peptides, less phosphate was released when phosphorylated Ser229 was used as a substrate (Figure 17B). To get an idea of the general dephosphorylation trend, we incubated fixed concentrations of one of the three myotilin phospho-peptides with CN and stopped the reaction at different time points. Our preliminary data suggest that at a timepoint where other reactions seem to be reaching saturation, the reaction involving the peptide bearing phosphorylated S229 is still developing and the signal detected is approximately three times lower compared to the other reactions (Figure 17C). Although there are fine differences in processing of the three phosphorylated serines, our data shows that myotilin is a substrate of CN and suggest that all three serines of interest, Ser229, Ser231 and Ser233, are *in vitro* targets of CN.

Identifying a counterpart of CN, one or multiple kinases which phosphorylate these serines, could be a starting point in obtaining a deeper understanding of myotilin phosphorylation, its regulation and would help elucidate its importance in the context of the Z-disc and potentially Ca^{2+} signaling.

To find such kinase candidates, myotilin sequence was used as an input in a Scansite4.0 search. The search resulted in several kinase candidates, the highest being protein kinase B (AKT). Thus, we tested whether AKT was able to phosphorylate our myotilin. To perform the phosphorylation assay, a constitutively active kinase domain of AKT was incubated with different concentrations of the $Myot^{185-444}$ construct. Although the assay was repeated twice, the result remains inconclusive; due to high error values, high AKT basal activity, high signal of myotilin in the absence of AKT and inconsistency between the two measurements it is not clear weather myotilin is phosphorylated by AKT. Thus, we could not conclude that myotilin is a substrate of AKT (Figure 18).

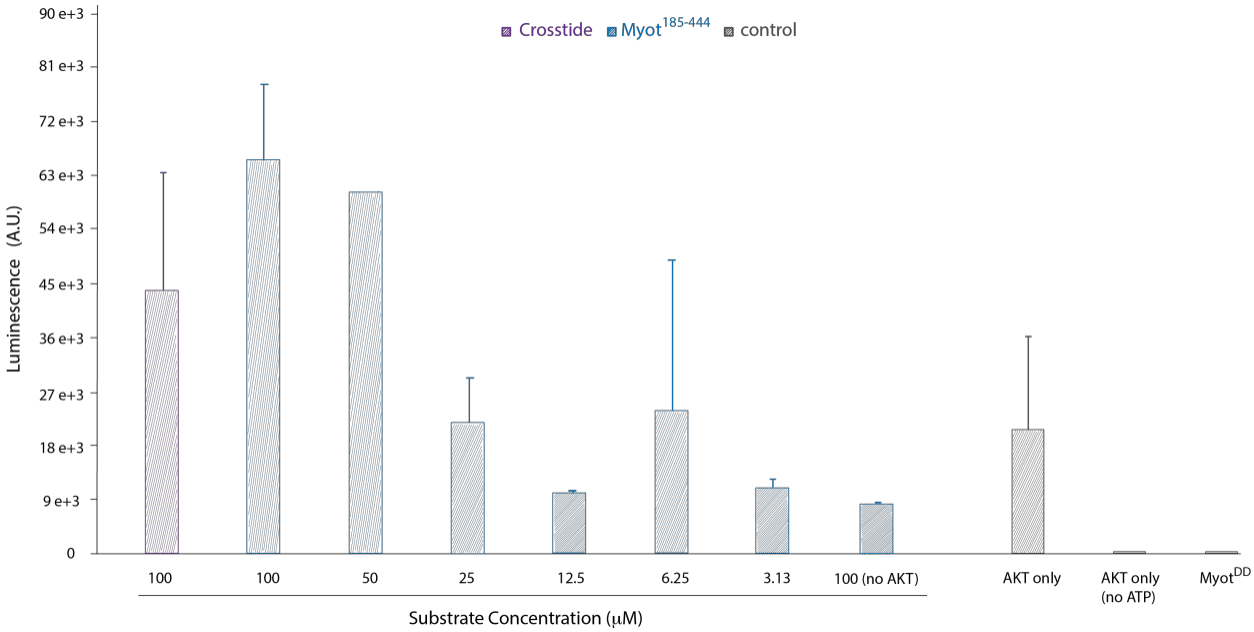

Figure 18. Phosphorylation assay to test phosphorylation of myotilin by AKT.

Phosphorylation assay to test whether $Myot^{185-444}$ is a substrate of AKT. As positive control, the established AKT substrate, a Crosstide peptide was used. The Crosstide peptide was phosphorylated, indicating that the AKT was active. Different $Myot^{185-444}$ concentrations were incubated with AKT to test its phosphorylation: although phosphorylation was detected in the wells containing two highest concentrations of $Myot^{185-444}$, the signal measured for lower concentrations of $Myot^{185-444}$ fluctuate, and the phosphorylation does not seem to be dependent on $Myot^{185-444}$ concentration. Additionally, wells containing two of the four negative controls, namely $Myot^{185-444}$ alone or AKT alone in the reaction buffer, have high basal activity. Finally, there was no signal detected when AKT was incubated in a buffer without ATP or when AKT was incubated in the standard reaction buffer, but instead of $Myot^{185-444}$, a myotilin construct containing a double phosphomimetic mutation (S229D and S233D) was used instead as a negative control.

Discussion

Myotilin has always played an important role in the Z-disc assembly, as one of the main actin organizing proteins. It has always been a powerful driving force of research, since its malfunction is linked to severe pathologies of the muscle tissue. This scaffolding protein however, might be more dynamic than originally thought; myotilin interacts with multiple Z-disc proteins and its stability is regulated by calpain and MURF-1, two proteins which are active in major Ca^{2+}-driven signal transduction pathways. Through its interaction to FATZ, myotilin has indirectly been linked to CN, a Ca^{2+}-dependent phosphatase which mediates muscle fiber type switching, muscle repair and growth as well as muscle degradation. In this study, we shown that myotilin directly interacts with CN, we characterize this interaction using structural and biophysical methods and lastly, we identify myotilin as a novel substrate of CN. This is an important discovery both in the myotilin and CN field. In regard to myotilin, this discovery holds the potential to, if supported through further investigation, elucidate molecular mechanisms of myotilin regulation. Which respect to the CN field, our finding expands the limited pool of identified CN binding partners. In addition, characterization of the myotilin-CN interaction could serve as a useful tool for conformation or validation of what is speculated or known about CN substrates.

On calcineurin stability

In our work we employ multiple techniques including pull-down and the peptide array assay, SEC-MALS, ITC, X-ray crystallography and CN activity assay to perform a detailed investigation of the CN-myotilin interaction. This was somewhat challenging at times the protein seemed to be unstable and prone to unspecific oligomerization once frozen, as confirmed by our DLS measurements. Thus, we prepared a fresh batch of protein for every experiment we performed. Even then, we found that the protein could not be concentrated to high values, our SEC-MALS profile of CN showed a small peak of molecular weight higher than expected and the number of binding sites as assessed by ITC was 0.5 or less. Arguably, modifying the construct to increase its stability, could ease the biochemical and biophysical characterization of the CN-myotilin interaction. Additionally, although we solved the structure of the complex at 2.77 Å, which allows us to determine both CN and myotilin residues responsible for binding, a complex with improved stability could also lead to increse in resolution. A way to obtain a more stable CN construct could be through CN myristoylation. It has been reported previously that N-terminal myristoylation of the CNB influences CN stability and increases its melting temperature by approximately 10° C in a thermal shift assay (Kennedy et al., 1996). Although it is disputed whether this modification decreases enzyme's activity, (Connolly and Kingsbury, 2012; Kennedy et al., 1996), such CN construct could certainly be used for non-activity-based experiments, given that substrate binding remains unaffected.

On identifying myotilin as a binding partner of calcineurin

Using pull-down experiments, we showed that CN and myotilin interact and found the region between residues 185 and 250 of myotilin to be responsible for CN binding. We further narrowed down this region and identified the LxVP CN binding motif of myotilin, using CelluSpots. Interestingly, although a recent study defined less stringent criteria to identify 567 potential new targets of CN, 45 of them in muscle tissues, this pool of candidates did not include myotilin (Sheftic

et al., 2016). Myotilin satisfies the first two conditions used for this search, namely its CN binding motif is found in a disordered region and it possesses confirmed pSer or pThr residues, however, it fails to fulfil the other two major requirements (Sheftic et al., 2016). Firstly, myotilin does not contain PxIxIT motif, which is the second short linear motif (SLiM) recognized by CN (Park et al., 2000). This is not atypical, since multiple studies have reported CN binding partners, which contain only one of the two established CN binding motifs (Czirjak and Enyedi, 2014; Sheftic et al., 2016). Secondly, the authors expand the LxVP motif to define a new, less strict p-f-L-x-(VPL)-(PK) motif, where p is a polar and f a polar residue capable of establishing a hydrogen bond. Interestingly, the LxVP motif on myotilin has an Ala and an Arg residue at the position corresponding to p and f, respectively. Although expanding the canonically accepted LxVP motif helped identify new potential members of the CN interactome (Sheftic et al., 2016), it also prevented the identification of others like myotilin. This also emphasizes the importance of characterizing new CN binders, to improve the search model in hopes of finding other CN substrates and regulators.

On the myotilin-calcineurin interaction

While it failed to identify myotilin as a CN binder, the newly defined π-ϕ-L-x-(VPL)-(PK) motif, along with our crystal structure, makes it easier to understand the subtle differences between binding affinity of myotilin compared to some other CN substrates. Our crystal structure confirmed that the LxVP motif of CN is indeed responsible for interacting with CN. Interestingly, previously reported crystal structures of CN in complex with its substrate NFATc1 or its inhibitor A238L both show additional interactions which further stabilize these complexes. Namely, a hydrophobic residue at position -1 (the π residue from the motif) and a polar residue at -2 (the ϕ residue) which form a hydrogen network with the Gln50 residue of CNB. Even though the dissociation constant of 6 µM measured for CN-myotilin binding is in good agreement with other LxVP bearing substrates, which bind CN with affinities in the lower µM range, it was shown that mutating -1 and -2 positioned residues relative to the LXVP motif could result in an increase of binding affinity (REF). Additionally, core residues of the LxVP motif could also be specifically altered to either enhance or diminish CN binding (Czirjak and Enyedi, 2014; Sheftic et al., 2016). Constructs Myot$^{185-444}$ R219Y Q221A and Myot$^{185-444}$ V222A P223A have already been cloned and purified, but not used due to time restraints. These could easily be used in the future to validate and extend our findings from the pull-down, ITC or SEC-MALS experiments.

On the metal calcineurin active center in our structure

The structure of CN, which we report in this work, is highly similar to previously reported structures of CN. Notably, only around 20% of the PDB deposited CN structures contain Zn or Fe metal ions in the active site, and only for 3 (around 5%) of these structures a comment was given on why these ions were included. According to the publications which describe these three structures, namely 1tco (Griffith et al., 1995), 1m63 (Huai et al., 2002) and 1aui (Kissinger et al., 1995), metals were modelled without experimental validation, based on similarity to the active center of purple acid phosphatase (Griffith et al., 1995, Kissinger et al., 1995) and by referring to previously conducted studies, where spectroscopic and kinetic analysis was performed to characterize the active site of CN (King and Huang, 1984; Mertz et al., 1997). King and Huang (1984) reported that Zn and Fe bind in a nondissociable manner to the active site of CN. Along with Ca^{2+} ions which bind to CNB to stabilize the overall CN fold, King and Huang (1984) have shown that other divalent ions

like Ni^{2+}, Mn^{2+}, Co^{2+}, Zn^{2+} and Mg^{2+} increase the activity of CN; they suggested that they increase the activity by stabilizing CN through binding to an unknown binding site (King and Huang, 1984).

In our work, we showed CN successfully dephosphorylates the widely used pNPP compound and the standard CN substrate RII, showing that the enzyme we crystalised is active. X-ray fluorescence scan performed at ESRF on a crystal of CN-Myot$^{213-232}$ (not used for data-collection) did not show presence of any metals that have been previously found in the active site of CN structures.

Interestingly, the active site residues which coordinate metal ions overlap almost perfectly when our structure is aligned to previously solved structures deposited with or without metal ions in the active center (Figure 9C). Furthermore, we did observe difference electron density (up to 6.8 σ-level) at the active site of CN, but it was not corroborated by the σ_A-weighted $2mF_o–DF_c$ map and could not be explained by metal ions even with lower occupancies. Therefore, this might be a refinement artifact and we have not modelled any metal ions or other ligands in the CN active site of our structure.

On myotilin dephosphorylation by calcineurin

Having found and characterized the interaction between myotilin and CN, we strived to elucidate the nature of this interaction. Proteins which interact with CN are known to be either CN substrates, CN inhibitors or anchoring proteins which dictate CN localization to a specific cellular region (Li et al., 2011). Although myotilin contains the LxVP motif, which is most predominantly used as a substrate recognition motif (Czirjak and Enyedi, 2014; Li et al., 2011; Sheftic et al., 2016), several CN inhibitors, including enzyme's own autoinhibitory region, carry the LxVP motif and use it for CN deactivation. We were led to speculate that myotilin was rather a substrate than an inhibitor of CN, since we determined that the myotilin-CN dissociation constant is in the low µM range, which corresponded better to values reported for CN-substrate than CN-inhibitor complexes (Grigoriu et al., 2013). In our dephosphorylation assays, all three tested serine residues, Ser229, Ser231 and Ser233, were dephosphorylated by CN. Having shown this, it would now be of interest to investigate other potential phosphorylated sites of myotilin, primarily Thr232, which is the neighbor residue of Ser231 and Ser233.

Our preliminary results indicated that Ser229 was dephosphorylated at a lower rate than the other two phospho-serines. Although we could model pSer229 entering the active site (Figure 11), according to literature, phosphorylated residues found six or less residues away from the LxVP motif are not likely to be processed efficiently by CN. Consequently, we cannot conclude that Ser229 is a true substrate of CN. Moreover, to validate our dephosphorylation results, dephosphorylation assays should be performed in context of a full length myotilin proteins, as assays performed solely using phospho-peptides have reported to lead to a higher degree of false positive results (Fahs et al., 2016). Another question which remains to be answered is whether only one, two or all three of these serine residues can be phosphorylated at the time, especially in context of dephosphorylation efficiency. The presence of several substrates which are located so close to each other might enhance or impair the activity of the phosphatase. Finally, even if all three serines are dephosphorylated *in vitro*, dephosphorylation studies should also be carried out *in vivo*, to show which of these dephosphorylation events is physiologically relevant. Additionally, mutations which mimic phosphorylation like the serine to aspartic acid mutation, could be then

used *in vivo* to validate the finding and test the effect such mutations could have on the myotilin behavior in the context of the entire Z-disk.

On using myotilin for learning about calcineurin dephosphorylation mechanism in general

Myotilin is unique among LxVP bearing CN substrates, since it contains several phosphorylated residues very close to the CN binding site. This would make myotilin a suitable candidate for testing the speculated minimal distance a residue must have from the LxVP binding motif in order to be dephosphorylated by CN (Grigoriu et al., 2013). In addition, kinetic studies and competition assays could be performed to quantify subtle differences in phosphorylation rates of a particular residue as a function of its distance from the LxVP motif. Myotilin could also be used to obtain structural understanding of the general mechanism CN uses to dephosphorylate its substrates. Crystallization of either inactive CN with a phosphorylated myotilin peptide or an active CN with a peptide carrying a phospho-mimetic mutation could be attempted. As opposed to many other CN substrate which contain long disordered stretches between the LxVP motif and the phosphorylated target residue which would not be suitable for crystallization, myotilin would be a good choice for such experiment.

On the impact myotilin phosphorylation state might have on its interaction

Most prominently, our findings provoke thoughts of myotilin regulation in the context of the entire Z-disc. Myotilin is primarily known as a protein that maintains the organization of sarcomeres due to its F-actin binding ability and F-actin bundling potential (Salmikangas et al., 2003). Like some other actin binding proteins, it contains Ig-like domains which enable interaction with F-actin (Jin, 2000; Otey et al., 2009; Otey et al., 2005). Previous studies have suggested however, that the N- and the C-terminal regions flanking the Ig-like domains also play a role in establishing this interaction (von Nandelstadh et al., 2005), and more recently, the region spanning 30-40 residues located N-terminally of the first Ig-like domain was speculate to fine-tune and potentially regulate the F-actin-myotilin interaction (Kostan et al., unpublished). Strikingly, the LxVP motif of myotilin, as well as all three serine residues shown to be dephosphorylated by CN, are all found in this region. Consequently, our findings raise an interesting question about the role of CN in regulation of the myotilin interactome. Most prominently, myotilin phosphorylation pattern might influence its ability to bind or bundle F-actin, which could have an effect on the overall organization of F-actin and thus, the whole Z-disk. Additionally, as myotilin is known to interact with many other major Z-disc proteins, it is plausible to speculate that these interactions could also be regulated by the phosphorylation state of myotilin. This is not a new concept, since it has been reported previously that the interaction of myotilin with ZASP is regulated through myotilin phosphorylation by CaMKII and PKA (von Nandelstadh et al., 2009). Hence, it would be of great interest to investigate the impact myotilin dephosphorylation by CN would have in the *in vivo* environment. Recombinant myotilin, carrying mutations in the LxVP motif, which either abolish or enhance the interaction, or myotilin construct that carry phospho-mimetic mutations and are for that reason not susceptible to dephosphorylation, could be used to get a deeper understanding of the role CN-mediated regulation on myotilin has on the its scaffolding function in the Z-disc.

On CN-mediated regulation of myotilin dynamics

We speculate that myotilin dephosphorylation could trigger its turnover or affect its role in muscle remodeling. Apart from bearing the LxVP motif and the three phosphorylated serines, the aforementioned 30 amino acid long stretch, which resides N-terminally of the first Ig-like domain, also contains a calpain cleavage motif as well as a ubiquitination site. Therefore, we propose that this region could be a hotspot of myotilin regulation (Figure 19). Myotilin is a target of calpain, a key Ca^{2+}-deriven protease of the muscle, activated together with CN, which cleaves muscle proteins to promote muscle remodeling and protein degradation (von Nandelstadh et al., 2011). Interestingly, it was recently shown that cleavage of Filamin-C, another Z-disc target of calpain, is less efficient when a residue in proximity of the cleavage site is phosphorylated (Reimann et al., 2017). The same might be true for myotilin, since its calpain cleavage site is located in the short region between the LxVP motif and the three phosphorylated serines. This emphasizes the importance of finding the kinase, which would potentially prevent the cleavage, making it an important factor in maintenance of myotilin homeostasis. To date, the only two kinases known to interact with myotilin, namely CaMKII and PKA, are only reported to phosphorylate a Ser residue at its C-terminus and our attempt to identify Akt as a potential myotilin kinase remained inconclusive. While phosphorylation would protect myotilin from being degraded, CN mediated dephosphorylation would promote myotilin cleavage by calpain. This cleavage would result in separation of the N-terminal disordered half of myotilin, that interact with α-actinin, from the two Ig-like domains, which bind F-actin. Since the cleavage site resides in the part of myotilin speculated to support F-actin binding, this could also lead to a decrease in myotilin's affinity to F-actin.

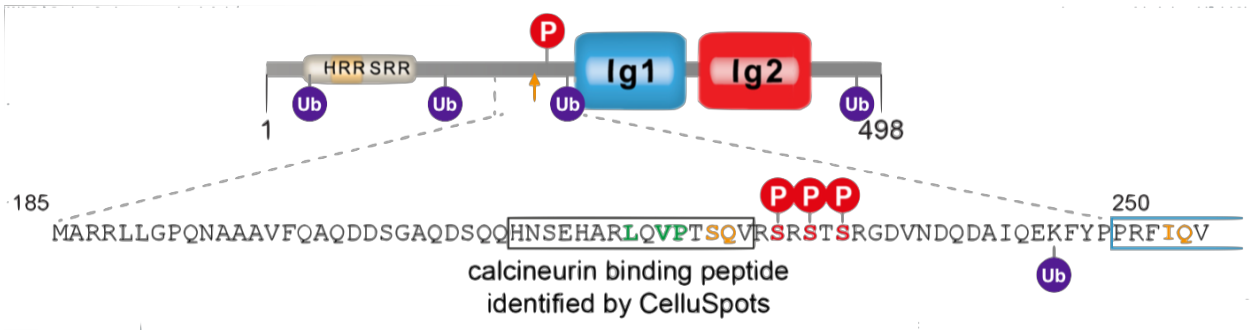

Figure 19. Myotilin region between residue 220 and 250 could be a hotspot of its regulation.

Myotilin contains the LxVP motif (green), three phosphorylated serine residues (red), two calpain cleavage sites (orange) and a ubiquitination site (purple), all concentrated in the short region between residues 220 and 250, located just before the first Ig-like domain.

Furthermore, a lysine in this region, namely Lys246, is supposed to be ubiquitinated. Although no studies were done to investigate which protein is responsible for ubiquitination of this exact site, it is known that the muscle specific E3 ligase MuRF-1 interacts with myotilin (Witt et al., 2005). MuRF-1 expression was recently reported to be elevated upon CN activation, as CN dephosphorylates FoxO, the transcription factor responsible for upregulation of MURF-1 transcription (Shimizu et al., 2017).

Finally, there is some indication that myotilin could act as a marker of muscle remodeling in muscle lesions caused by DOMS and eccentric exercise. Such lesions are not rich in α-actinin or desmin, which were originally linked to muscle remodeling, but contain high amounts of F-actin bound myotilin. Myotilin is speculated to drive sarcomere lengthening and repair, by recruitment of

monomeric G-actin (Carlsson et al., 2007). Although Ca^{2+} concentration is only temporary increased upon eccentric exercise, CN is transiently activated regulate repair and rebuilding of the muscle (MacNeil et al., 2010). This could be another important process, in which CN could influence myotilin dynamic and thus, its behavior during muscle remodeling.

Abbreviations

3C protease	Human rhinovirus 3C protease
Calmodulin	CaM
CaMK	calcium/calmodulin-dependent kinase
CN	calcineurin
CNA	calcineurin subunit A
CNB	Calcineurin subunit B
DTT	dithiothreitol
EDTA	ethylenediaminetetraacetic acid
IPTG	sopropyl-β-D-Thiogalactopyranoside
ITC	isothermal titration calorimetry
MLP	muscle LIM protein
MURF-1	muscle RING-finger protein-1
Myot	myotilin
OD_{600}	optical density at 600 nm
PKA	Protein kinase A
PMSF	phenylmethane sulfonyl fluoride
pSer	phhosphorylated serine
SLS	static light scattering
TCEP	2-carboxyethyl-phosphine
TEMED	Tetramethylethylenediamine
TEV protease	tobacco etch virus
Tris	Tris(hydroxymethyl)aminomethane

References

Adams, P.D., Afonine, P.V., Bunkoczi, G., Chen, V.B., Davis, I.W., Echols, N., Headd, J.J., Hung, L.W., Kapral, G.J., Grosse-Kunstleve, R.W., *et al.* (2010). PHENIX: a comprehensive Python-based system for macromolecular structure solution. Acta Crystallogr D Biol Crystallogr *66*, 213-221.

Aramburu, J., Garcia-Cozar, F., Raghavan, A., Okamura, H., Rao, A., and Hogan, P.G. (1998). Selective inhibition of NFAT activation by a peptide spanning the calcineurin targeting site of NFAT. Mol Cell *1*, 627-637.

Aramburu, J., Rao, A., and Klee, C.B. (2000). Calcineurin: from structure to function. Curr Top Cell Regul *36*, 237-295.

Azzi, J.R., Sayegh, M.H., and Mallat, S.G. (2013). Calcineurin inhibitors: 40 years later, can't live without. J Immunol *191*, 5785-5791.

Bang, M.L., Mudry, R.E., McElhinny, A.S., Trombitas, K., Geach, A.J., Yamasaki, R., Sorimachi, H., Granzier, H., Gregorio, C.C., and Labeit, S. (2001). Myopalladin, a novel 145-kilodalton sarcomeric protein with multiple roles in Z-disc and I-band protein assemblies. J Cell Biol *153*, 413-427.

Bassel-Duby, R., and Olson, E.N. (2006). Signaling pathways in skeletal muscle remodeling. Annu Rev Biochem *75*, 19-37.

Beck, M.R., Otey, C.A., and Campbell, S.L. (2011). Structural characterization of the interactions between palladin and alpha-actinin. J Mol Biol *413*, 712-725.

Berridge, M.J., Lipp, P., and Bootman, M.D. (2000). The versatility and universality of calcium signalling. Nat Rev Mol Cell Biol *1*, 11-21.

Beto, J.A. (2015). The role of calcium in human aging. Clin Nutr Res *4*, 1-8.

Blanchard, A., Ohanian, V., and Critchley, D. (1989). The structure and function of alpha-actinin. J Muscle Res Cell Motil *10*, 280-289.

Bootman, M.D. (2012). Calcium signaling. Cold Spring Harb Perspect Biol *4*, a011171.

Boss, V., Abbott, K.L., Wang, X.F., Pavlath, G.K., and Murphy, T.J. (1998). The cyclosporin A-sensitive nuclear factor of activated T cells (NFAT) proteins are expressed in vascular smooth muscle cells. Differential localization of NFAT isoforms and induction of NFAT-mediated transcription by phospholipase C-coupled cell surface receptors. J Biol Chem *273*, 19664-19671.

Caraveo, G., Soste, M., Cappelleti, V., Fanning, S., van Rossum, D.B., Whitesell, L., Huang, Y., Chung, C.Y., Baru, V., Zaichick, S., *et al.* (2017). FKBP12 contributes to alpha-synuclein toxicity by regulating the calcineurin-dependent phosphoproteome. Proc Natl Acad Sci U S A *114*, E11313-E11322.

Carlsson, L., Yu, J.G., Moza, M., Carpen, O., and Thornell, L.E. (2007). Myotilin: a prominent marker of myofibrillar remodelling. Neuromuscul Disord *17*, 61-68.

Casella, J.F., Maack, D.J., and Lin, S. (1986). Purification and initial characterization of a protein from skeletal muscle that caps the barbed ends of actin filaments. J Biol Chem *261*, 10915-10921.

Chen, V.B., Arendall, W.B., 3rd, Headd, J.J., Keedy, D.A., Immormino, R.M., Kapral, G.J., Murray, L.W., Richardson, J.S., and Richardson, D.C. (2010). MolProbity: all-atom structure validation for macromolecular crystallography. Acta Crystallogr D Biol Crystallogr *66*, 12-21.

Chin, E.R., Olson, E.N., Richardson, J.A., Yang, Q., Humphries, C., Shelton, J.M., Wu, H., Zhu, W., Bassel-Duby, R., and Williams, R.S. (1998). A calcineurin-dependent transcriptional pathway controls skeletal muscle fiber type. Genes Dev *12*, 2499-2509.

Clapham, D.E. (2007). Calcium signaling. Cell *131*, 1047-1058.

Czirjak, G., and Enyedi, P. (2014). The LQLP calcineurin docking site is a major determinant of the calcium-dependent activation of human TRESK background K+ channel. J Biol Chem *289*, 29506-29518.

Dayton, W.R., Goll, D.E., Zeece, M.G., Robson, R.M., and Reville, W.J. (1976). A Ca2+-activated protease possibly involved in myofibrillar protein turnover. Purification from porcine muscle. Biochemistry *15*, 2150-2158.

Delling, U., Tureckova, J., Lim, H.W., De Windt, L.J., Rotwein, P., and Molkentin, J.D. (2000). A calcineurin-NFATc3-dependent pathway regulates skeletal muscle differentiation and slow myosin heavy-chain expression. Mol Cell Biol *20*, 6600-6611.
Emal, D., Rampanelli, E., Claessen, N., Bemelman, F.J., Leemans, J.C., Florquin, S., and Dessing, M.C. (2019). Calcineurin inhibitor Tacrolimus impairs host immune response against urinary tract infection. Sci Rep *9*, 106.
Emsley, P., Lohkamp, B., Scott, W.G., and Cowtan, K. (2010). Features and development of Coot. Acta Crystallogr D Biol Crystallogr *66*, 486-501.
Fahs, S., Lujan, P., and Kohn, M. (2016). Approaches to Study Phosphatases. ACS Chem Biol *11*, 2944-2961.
Faul, C., Dhume, A., Schecter, A.D., and Mundel, P. (2007). Protein kinase A, Ca2+/calmodulin-dependent kinase II, and calcineurin regulate the intracellular trafficking of myopodin between the Z-disc and the nucleus of cardiac myocytes. Mol Cell Biol *27*, 8215-8227.
Faulkner, G., Pallavicini, A., Formentin, E., Comelli, A., Ievolella, C., Trevisan, S., Bortoletto, G., Scannapieco, P., Salamon, M., Mouly, V.*, et al.* (1999). ZASP: a new Z-band alternatively spliced PDZ-motif protein. J Cell Biol *146*, 465-475.
Frank, D., and Frey, N. (2011). Cardiac Z-disc signaling network. J Biol Chem *286*, 9897-9904.
Frank, D., Kuhn, C., Katus, H.A., and Frey, N. (2006). The sarcomeric Z-disc: a nodal point in signalling and disease. J Mol Med (Berl) *84*, 446-468.
Frey, N., Richardson, J.A., and Olson, E.N. (2000). Calsarcins, a novel family of sarcomeric calcineurin-binding proteins. Proc Natl Acad Sci U S A *97*, 14632-14637.
Friday, B.B., Mitchell, P.O., Kegley, K.M., and Pavlath, G.K. (2003). Calcineurin initiates skeletal muscle differentiation by activating MEF2 and MyoD. Differentiation *71*, 217-227.
Frontera, W.R., and Ochala, J. (2015). Skeletal muscle: a brief review of structure and function. Calcif Tissue Int *96*, 183-195.
Garvey, S.M., Miller, S.E., Claflin, D.R., Faulkner, J.A., and Hauser, M.A. (2006). Transgenic mice expressing the myotilin T57I mutation unite the pathology associated with LGMD1A and MFM. Hum Mol Genet *15*, 2348-2362.
Gautel, M., and Djinovic-Carugo, K. (2016). The sarcomeric cytoskeleton: from molecules to motion. J Exp Biol *219*, 135-145.
Gehlert, S., Bloch, W., and Suhr, F. (2015). Ca2+-dependent regulations and signaling in skeletal muscle: from electro-mechanical coupling to adaptation. Int J Mol Sci *16*, 1066-1095.
Gontier, Y., Taivainen, A., Fontao, L., Sonnenberg, A., van der Flier, A., Carpen, O., Faulkner, G., and Borradori, L. (2005). The Z-disc proteins myotilin and FATZ-1 interact with each other and are connected to the sarcolemma via muscle-specific filamins. J Cell Sci *118*, 3739-3749.
Goy, J.J., Stauffer, J.C., Deruaz, J.P., Gillard, D., Kaufmann, U., Kuntzer, T., and Kappenberger, L. (1989). Myopathy as possible side-effect of cyclosporin. Lancet *1*, 1446-1447.
Griffith, J.P., Kim, J.L., Kim, E.E., Sintchak, M.D., Thomson, J.A., Fitzgibbon, M.J., Fleming, M.A., Caron, P.R., Hsiao, K., and Navia, M.A. (1995). X-ray structure of calcineurin inhibited by the immunophilin-immunosuppressant FKBP12-FK506 complex. Cell *82*, 507-522.
Grigoriu, S., Bond, R., Cossio, P., Chen, J.A., Ly, N., Hummer, G., Page, R., Cyert, M.S., and Peti, W. (2013). The molecular mechanism of substrate engagement and immunosuppressant inhibition of calcineurin. PLoS Biol *11*, e1001492.
Hauser, M.A., Horrigan, S.K., Salmikangas, P., Torian, U.M., Viles, K.D., Dancel, R., Tim, R.W., Taivainen, A., Bartoloni, L., Gilchrist, J.M.*, et al.* (2000). Myotilin is mutated in limb girdle muscular dystrophy 1A. Hum Mol Genet *9*, 2141-2147.
Heikkinen, O., Permi, P., Koskela, H., Carpen, O., Ylanne, J., and Kilpelainen, I. (2009). Solution structure of the first immunoglobulin domain of human myotilin. J Biomol NMR *44*, 107-112.

Heineke, J., Wollert, K.C., Osinska, H., Sargent, M.A., York, A.J., Robbins, J., and Molkentin, J.D. (2010). Calcineurin protects the heart in a murine model of dilated cardiomyopathy. J Mol Cell Cardiol *48*, 1080-1087.
Huai, Q., Kim, H.Y., Liu, Y., Zhao, Y., Mondragon, A., Liu, J.O., and Ke, H. (2002). Crystal structure of calcineurin-cyclophilin-cyclosporin shows common but distinct recognition of immunophilin-drug complexes. Proc Natl Acad Sci U S A *99*, 12037-12042.
Hudson, M.B., and Price, S.R. (2013). Calcineurin: a poorly understood regulator of muscle mass. Int J Biochem Cell Biol *45*, 2173-2178.
Iwamoto, D.V., Huehn, A., Simon, B., Huet-Calderwood, C., Baldassarre, M., Sindelar, C.V., and Calderwood, D.A. (2018). Structural basis of the filamin A actin-binding domain interaction with F-actin. Nat Struct Mol Biol *25*, 918-927.
Jin, J.P. (2000). Titin-thin filament interaction and potential role in muscle function. Adv Exp Med Biol *481*, 319-333; discussion 334-315.
Jin, J.P., and Wang, K. (1991). Nebulin as a giant actin-binding template protein in skeletal muscle sarcomere. Interaction of actin and cloned human nebulin fragments. FEBS Lett *281*, 93-96.
King, M.M., and Huang, C.Y. (1984). The calmodulin-dependent activation and deactivation of the phosphoprotein phosphatase, calcineurin, and the effect of nucleotides, pyrophosphate, and divalent metal ions. Identification of calcineurin as a Zn and Fe metalloenzyme. J Biol Chem *259*, 8847-8856.
Kissinger, C.R., Parge, H.E., Knighton, D.R., Lewis, C.T., Pelletier, L.A., Tempczyk, A., Kalish, V.J., Tucker, K.D., Showalter, R.E., Moomaw, E.W.*, et al.* (1995). Crystal structures of human calcineurin and the human FKBP12-FK506-calcineurin complex. Nature *378*, 641-644.
Kuo, I.Y., and Ehrlich, B.E. (2015). Signaling in muscle contraction. Cold Spring Harb Perspect Biol *7*, a006023.
Lara-Pezzi, E., Winn, N., Paul, A., McCullagh, K., Slominsky, E., Santini, M.P., Mourkioti, F., Sarathchandra, P., Fukushima, S., Suzuki, K.*, et al.* (2007). A naturally occurring calcineurin variant inhibits FoxO activity and enhances skeletal muscle regeneration. J Cell Biol *179*, 1205-1218.
Lee, H.J., and Zheng, J.J. (2010). PDZ domains and their binding partners: structure, specificity, and modification. Cell Commun Signal *8*, 8.
Li, H., Rao, A., and Hogan, P.G. (2004). Structural delineation of the calcineurin-NFAT interaction and its parallels to PP1 targeting interactions. J Mol Biol *342*, 1659-1674.
Li, H., Rao, A., and Hogan, P.G. (2011). Interaction of calcineurin with substrates and targeting proteins. Trends Cell Biol *21*, 91-103.
Li, H., Zhang, L., Rao, A., Harrison, S.C., and Hogan, P.G. (2007). Structure of calcineurin in complex with PVIVIT peptide: portrait of a low-affinity signalling interaction. J Mol Biol *369*, 1296-1306.
Lin, C., Guo, X., Lange, S., Liu, J., Ouyang, K., Yin, X., Jiang, L., Cai, Y., Mu, Y., Sheikh, F.*, et al.* (2013). Cypher/ZASP is a novel A-kinase anchoring protein. J Biol Chem *288*, 29403-29413.
Lin, X., Ruiz, J., Bajraktari, I., Ohman, R., Banerjee, S., Gribble, K., Kaufman, J.D., Wingfield, P.T., Griggs, R.C., Fischbeck, K.H.*, et al.* (2014). Z-disc-associated, alternatively spliced, PDZ motif-containing protein (ZASP) mutations in the actin-binding domain cause disruption of skeletal muscle actin filaments in myofibrillar myopathy. J Biol Chem *289*, 13615-13626.
MacNeil, L.G., Melov, S., Hubbard, A.E., Baker, S.K., and Tarnopolsky, M.A. (2010). Eccentric exercise activates novel transcriptional regulation of hypertrophic signaling pathways not affected by hormone changes. PLoS One *5*, e10695.
Mertz, P., Yu, L., Sikkink, R., and Rusnak, F. (1997). Kinetic and spectroscopic analyses of mutants of a conserved histidine in the metallophosphatases calcineurin and lambda protein phosphatase. J Biol Chem *272*, 21296-21302.
Moza, M., Mologni, L., Trokovic, R., Faulkner, G., Partanen, J., and Carpen, O. (2007). Targeted deletion of the muscular dystrophy gene myotilin does not perturb muscle structure or function in mice. Mol Cell Biol *27*, 244-252.

Nave, R., Furst, D.O., and Weber, K. (1990). Interaction of alpha-actinin and nebulin in vitro. Support for the existence of a fourth filament system in skeletal muscle. FEBS Lett *269*, 163-166.
Olson, E.N., and Williams, R.S. (2000). Remodeling muscles with calcineurin. Bioessays *22*, 510-519.
Otey, C.A., Dixon, R., Stack, C., and Goicoechea, S.M. (2009). Cytoplasmic Ig-domain proteins: cytoskeletal regulators with a role in human disease. Cell Motil Cytoskeleton *66*, 618-634.
Otey, C.A., Rachlin, A., Moza, M., Arneman, D., and Carpen, O. (2005). The palladin/myotilin/myopalladin family of actin-associated scaffolds. Int Rev Cytol *246*, 31-58.
Parast, M.M., and Otey, C.A. (2000). Characterization of palladin, a novel protein localized to stress fibers and cell adhesions. J Cell Biol *150*, 643-656.
Park, S., Uesugi, M., and Verdine, G.L. (2000). A second calcineurin binding site on the NFAT regulatory domain. Proc Natl Acad Sci U S A *97*, 7130-7135.
Pineda, J.R., Pardo, R., Zala, D., Yu, H., Humbert, S., and Saudou, F. (2009). Genetic and pharmacological inhibition of calcineurin corrects the BDNF transport defect in Huntington's disease. Mol Brain *2*, 33.
Puz, V., Pavsic, M., Lenarcic, B., and Djinovic-Carugo, K. (2017). Conformational plasticity and evolutionary analysis of the myotilin tandem Ig domains. Sci Rep *7*, 3993.
Reese, L.C., and Taglialatela, G. (2011). A role for calcineurin in Alzheimer's disease. Curr Neuropharmacol *9*, 685-692.
Reimann, L., Wiese, H., Leber, Y., Schwable, A.N., Fricke, A.L., Rohland, A., Knapp, B., Peikert, C.D., Drepper, F., van der Ven, P.F.*, et al.* (2017). Myofibrillar Z-discs Are a Protein Phosphorylation Hot Spot with Protein Kinase C (PKCalpha) Modulating Protein Dynamics. Mol Cell Proteomics *16*, 346-367.
Ribeiro Ede, A., Jr., Pinotsis, N., Ghisleni, A., Salmazo, A., Konarev, P.V., Kostan, J., Sjoblom, B., Schreiner, C., Polyansky, A.A., Gkougkoulia, E.A.*, et al.* (2014). The structure and regulation of human muscle alpha-actinin. Cell *159*, 1447-1460.
Rodriguez, A., Roy, J., Martinez-Martinez, S., Lopez-Maderuelo, M.D., Nino-Moreno, P., Orti, L., Pantoja-Uceda, D., Pineda-Lucena, A., Cyert, M.S., and Redondo, J.M. (2009). A conserved docking surface on calcineurin mediates interaction with substrates and immunosuppressants. Mol Cell *33*, 616-626.
Rumi-Masante, J., Rusinga, F.I., Lester, T.E., Dunlap, T.B., Williams, T.D., Dunker, A.K., Weis, D.D., and Creamer, T.P. (2012). Structural basis for activation of calcineurin by calmodulin. J Mol Biol *415*, 307-317.
Rusnak, F., and Mertz, P. (2000). Calcineurin: form and function. Physiol Rev *80*, 1483-1521.
Sakuma, K., Nishikawa, J., Nakao, R., Watanabe, K., Totsuka, T., Nakano, H., Sano, M., and Yasuhara, M. (2003). Calcineurin is a potent regulator for skeletal muscle regeneration by association with NFATc1 and GATA-2. Acta Neuropathol *105*, 271-280.
Sakuma, K., and Yamaguchi, A. (2010). The functional role of calcineurin in hypertrophy, regeneration, and disorders of skeletal muscle. J Biomed Biotechnol *2010*, 721219.
Salmikangas, P., Mykkanen, O.M., Gronholm, M., Heiska, L., Kere, J., and Carpen, O. (1999). Myotilin, a novel sarcomeric protein with two Ig-like domains, is encoded by a candidate gene for limb-girdle muscular dystrophy. Hum Mol Genet *8*, 1329-1336.
Salmikangas, P., van der Ven, P.F., Lalowski, M., Taivainen, A., Zhao, F., Suila, H., Schroder, R., Lappalainen, P., Furst, D.O., and Carpen, O. (2003). Myotilin, the limb-girdle muscular dystrophy 1A (LGMD1A) protein, cross-links actin filaments and controls sarcomere assembly. Hum Mol Genet *12*, 189-203.
Schiaffino, S., and Reggiani, C. (2011). Fiber types in mammalian skeletal muscles. Physiol Rev *91*, 1447-1531.
Selcen, D. (2008). Myofibrillar myopathies. Curr Opin Neurol *21*, 585-589.
Selcen, D., and Engel, A.G. (2004). Mutations in myotilin cause myofibrillar myopathy. Neurology *62*, 1363-1371.
Seto, J.T., Quinlan, K.G., Lek, M., Zheng, X.F., Garton, F., MacArthur, D.G., Hogarth, M.W., Houweling, P.J., Gregorevic, P., Turner, N.*, et al.* (2013). ACTN3 genotype influences muscle performance through the regulation of calcineurin signaling. J Clin Invest *123*, 4255-4263.

Shadrin, I.Y., Khodabukus, A., and Bursac, N. (2016). Striated muscle function, regeneration, and repair. Cell Mol Life Sci *73*, 4175-4202.
Shaw, K.T., Ho, A.M., Raghavan, A., Kim, J., Jain, J., Park, J., Sharma, S., Rao, A., and Hogan, P.G. (1995). Immunosuppressive drugs prevent a rapid dephosphorylation of transcription factor NFAT1 in stimulated immune cells. Proc Natl Acad Sci U S A *92*, 11205-11209.
Sheftic, S.R., Page, R., and Peti, W. (2016). Investigating the human Calcineurin Interaction Network using the piLxVP SLiM. Sci Rep *6*, 38920.
Shimizu, H., Langenbacher, A.D., Huang, J., Wang, K., Otto, G., Geisler, R., Wang, Y., and Chen, J.N. (2017). The Calcineurin-FoxO-MuRF1 signaling pathway regulates myofibril integrity in cardiomyocytes. Elife *6*.
Shizuta, Y., Shizuta, H., Gallo, M., Davies, P., and Pastan, I. (1976). Purification and properties of filamin, and actin binding protein from chicken gizzard. J Biol Chem *251*, 6562-6567.
Stupka, N., Schertzer, J.D., Bassel-Duby, R., Olson, E.N., and Lynch, G.S. (2007). Calcineurin-A alpha activation enhances the structure and function of regenerating muscles after myotoxic injury. Am J Physiol Regul Integr Comp Physiol *293*, R686-694.
Sussman, M.A., Lim, H.W., Gude, N., Taigen, T., Olson, E.N., Robbins, J., Colbert, M.C., Gualberto, A., Wieczorek, D.F., and Molkentin, J.D. (1998). Prevention of cardiac hypertrophy in mice by calcineurin inhibition. Science *281*, 1690-1693.
Swoap, S.J., Hunter, R.B., Stevenson, E.J., Felton, H.M., Kansagra, N.V., Lang, J.M., Esser, K.A., and Kandarian, S.C. (2000). The calcineurin-NFAT pathway and muscle fiber-type gene expression. Am J Physiol Cell Physiol *279*, C915-924.
Tallis, J., James, R.S., and Seebacher, F. (2018). The effects of obesity on skeletal muscle contractile function. J Exp Biol *221*.
Tavi, P., and Westerblad, H. (2011). The role of in vivo Ca(2)(+) signals acting on Ca(2)(+)-calmodulin-dependent proteins for skeletal muscle plasticity. J Physiol *589*, 5021-5031.
Tu, M.K., and Borodinsky, L.N. (2014). Spontaneous calcium transients manifest in the regenerating muscle and are necessary for skeletal muscle replenishment. Cell Calcium *56*, 34-41.
Tu, M.K., Levin, J.B., Hamilton, A.M., and Borodinsky, L.N. (2016). Calcium signaling in skeletal muscle development, maintenance and regeneration. Cell Calcium *59*, 91-97.
van der Ven, P.F., Wiesner, S., Salmikangas, P., Auerbach, D., Himmel, M., Kempa, S., Hayess, K., Pacholsky, D., Taivainen, A., Schroder, R*., et al.* (2000). Indications for a novel muscular dystrophy pathway. gamma-filamin, the muscle-specific filamin isoform, interacts with myotilin. J Cell Biol *151*, 235-248.
von Nandelstadh, P., Gronholm, M., Moza, M., Lamberg, A., Savilahti, H., and Carpen, O. (2005). Actin-organising properties of the muscular dystrophy protein myotilin. Exp Cell Res *310*, 131-139.
von Nandelstadh, P., Ismail, M., Gardin, C., Suila, H., Zara, I., Belgrano, A., Valle, G., Carpen, O., and Faulkner, G. (2009). A class III PDZ binding motif in the myotilin and FATZ families binds enigma family proteins: a common link for Z-disc myopathies. Mol Cell Biol *29*, 822-834.
von Nandelstadh, P., Soliymani, R., Baumann, M., and Carpen, O. (2011). Analysis of myotilin turnover provides mechanistic insight into the role of myotilinopathy-causing mutations. Biochem J *436*, 113-121.
Wang, J., Dube, D.K., Mittal, B., Sanger, J.M., and Sanger, J.W. (2011). Myotilin dynamics in cardiac and skeletal muscle cells. Cytoskeleton (Hoboken) *68*, 661-670.
Winn, M.D., Ballard, C.C., Cowtan, K.D., Dodson, E.J., Emsley, P., Evans, P.R., Keegan, R.M., Krissinel, E.B., Leslie, A.G., McCoy, A*., et al.* (2011). Overview of the CCP4 suite and current developments. Acta Crystallogr D Biol Crystallogr *67*, 235-242.
Witt, S.H., Granzier, H., Witt, C.C., and Labeit, S. (2005). MURF-1 and MURF-2 target a specific subset of myofibrillar proteins redundantly: towards understanding MURF-dependent muscle ubiquitination. J Mol Biol *350*, 713-722.
Yang, S.A., and Klee, C.B. (2000). Low affinity Ca2+-binding sites of calcineurin B mediate conformational changes in calcineurin A. Biochemistry *39*, 16147-16154.

Young, P., Ferguson, C., Banuelos, S., and Gautel, M. (1998). Molecular structure of the sarcomeric Z-disk: two types of titin interactions lead to an asymmetrical sorting of alpha-actinin. EMBO J *17*, 1614-1624.